neuronal cells was detectable and inhibited by some typical secretase inhibitors and modulators. Thus, we provide a new platform for AD drug development, which might be applied to AD patient-specific iPS cell research.

Results

Differentiation of forebrain neurons from hiPS cells

Recently, forebrain neurons were successfully differentiated from mouse embryonic stem (ES) cells [7,8,9] and human ES and/or iPS cells [9,10,11]. The methods used for differentiation into spinal motor neurons and midbrain dopaminergic neurons required the morphogens retinoic acid (RA)/sonic hedgehog (SHH) and fibroblast growth factor 8 (FGF8)/SHH, respectively [11,12]. On the other hand, non-morphogens [10,11] or Lefty A and Dickkopf homolog 1 (Dkk1) [7,9] have been used for the induction of hiPS cells into forebrain neurons. Because amyloid plaques are observed in the cerebral cortex from the early stage of AD development [13], stem cells should be differentiated to at least forebrain neurons for *in vitro* assays in AD research.

We differentiated forebrain neurons from hiPS 253G4 cells, which were generated from human dermal fibroblasts using three reprogramming factors (Oct3/4, Sox2, and Klf4) [14], as described previously (Figure 1A) [12,15]. When neural stem cells were induced with Noggin and SB431542 for 17 days, we obtained cells that were positive for the neuroectodermal marker, Nestin (Figure 1B), as previously reported using human and monkey ES cells [15]. After culturing the cells with morphogen-free medium for days 17–24, Forkhead box G1 (Foxg1) expression was induced and Foxg1-positive cells were observed (Figure 1C, D) [11,15]. We also examined whether treatment with cyclopamine, an SHH inhibitor, increased the number of neurons presenting a glutamatergic phenotype as observed in mouse ES cells [8]. The expression level of vesicular glutamate transporter 1 (vGlut1), a glutamatergic marker, was not significantly increased by the addition of cyclopamine (final concentration 1 μM) from days 17 to 24 (data not shown). Therefore, we did not add cyclopamine in this period in subsequent experiments. At day 24, dissociated cells were reseeded on 24-well plates to further characterize the cells.

Next, we evaluated the hiPS cell-derived neuronal cells using four cortical layer-specific markers, T-brain-1 (Tbr1) and chicken ovalbumin upstream promoter transcription factor (COUP-TF)-interacting protein 2 (Ctip2) [9,10,11], and cut-like homeobox 1 (Cux1) and special AT-rich sequence-binding protein 2 (Satb2) [16]. Quantitative polymerase chain reaction (qPCR) revealed that expression levels of these markers were increased in a differentiation day-dependent manner (Figure 1E). At day 52, all four of these markers were visualized by immunocytochemistry (ICC) (Figure 1F). The percentages of marker-positive cells relative to the total number of cells were 62.2±2.9% for Tbr1, 11.9±3.0% for Ctip2, 82.6±5.0% for Cux1, and46.0±7.1% for Satb2. The population of each marker-positive cell was similar to that of data reported previously in human fetal brain around gestational week-20 [16]. In this experimental schedule, most cells expressed one or a few neocortical markers at day 52.

Characterization of hiPS cell-derived neuronal cells

Cells that were reseeded at day 24, were sparsely adhered to the culture plate and had proliferated and extended neurites in a time course-dependent manner as observed by the neuronal marker, class-III β-tubulin (Tuj1), and microtubule-associated protein 2 (MAP2) (Figure 2A). Tuj1 expression was almost saturated at day 45 (Figure 2B), but MAP2 and synapsin I expression were still increasing (Figure 2C, D). Synaptic development continued until day 52, and many synapsin I-positive puncta were detected by ICC at day 52 (Figure 2A). Expression of the glial marker, glial fibrillary acidic protein (GFAP), was highest at day 52 in this schedule (Figure 2E). This sequential expression pattern is similar to that reported recently in human pluripotent stem cell-derived neurons; the synapsin I-positive neuronal and GFAP-positive glial cultures at day 52 corresponded to the stage at which spontaneous neuronal activity was observed [17].

We then examined the neurotransmitter phenotypes of these differentiated neurons by evaluating the synthesizing enzymes for two typical cortical neurotransmitters, glutamate and γ-aminobutyric acid (GABA). Expression of the glutamatergic neuronal marker, phosphate-activated glutaminase (PAG) [18], and the GABAergic neuronal marker, glutamate decarboxylase (GAD), were observed by ICC at day 52 (Figure 2F). PAG- and GAD-positive neurons comprised 60±20% and 5±4% of total cells, respectively. Most of the Tuj1-positive neurons were also co-localized with the punctate signals of vGlut1 (Figure 2G). GABA-positive neurons comprised a similar population to the GAD-positive ones (Figure 2F, H). On the other hand, cholineacetyltransferase (ChAT) or vesicular acetylcholine transporter (VAChT)-positive cholinergic neurons were little observed at day 52, although their mRNA level increased with differentiation time (Figure S1). These data showed that a majority of differentiated neuronal cells possessed a glutamatergic phenotype in the present condition.

Differentiated neuronal cells express some components related to Aβ production

To evaluate their usefulness as an AD model, we measured the levels of Aβ secreted from the differentiated neuronal cells at days 38, 45, and 52. In the non-amyloidogenic pathway, α-secretase cleaves full-length APP (FL-APP) within the Aβ domain to the large soluble APP fragment (sAPPα) and APP-C terminal fragment α (CTFα) (Figure 3) [19]. In the amyloidogenic pathway, β-secretase, β-site APP cleaving enzyme 1 (BACE1), cleaves APP on the N-terminal side of the Aβ domain to soluble sAPPβ and APP-CTFβ (Figure 3). FL-APP and its cleavage products were increased in a time-course-dependent manner (Figure 3).

APP has three alternatively spliced isoforms: APP695, APP751, and APP770. APP695 is most abundantly expressed in neurons, whereas APP751 and APP770 show more ubiquitous expression patterns [20]. In cell lysates, we detected three separate APP variants on western blots. The estimated percentages of the neuron-dominant variant APP695 were 64.5±1.0%, 68.6±2.2%, and 69.6±2.1% at days 38, 45, and 52, respectively (Figures 3A and S2). The neuronal population at day 52 was approximately consistent with the sum of the percentages of the glutamatergic and GABAergic neurons mentioned above.

The aspartyl protease BACE1, the major β-secretase involved in cleaving APP, is a significant molecule for AD pathology because BACE1 protein levels and activity are increased in the brains of patients with the sporadic form of AD [21]. In our differentiated neurons, BACE1 protein levels were increased in a time course-dependent manner (Figure 4A, B), and we speculated that the upregulation of BACE1 protein levels may be due to a posttranscriptional mechanism [22]. BACE1 mRNA levels were slightly elevated with time (Figure 4B). These data may indicate that increased BACE1 protein levels were mainly induced by translational activation along with neuronal differentiation.

APP-CTFβ is cleaved to Aβ and APP intercellular domain (AICD) by γ-secretase (Figure 3). The γ-secretase complex consists of four core members, presenilin (PS; either PS1 or PS2), nicastrin, Pen-2, and Aph-1 [23]. PS1, nicastrin, and Pen-2 were detected by

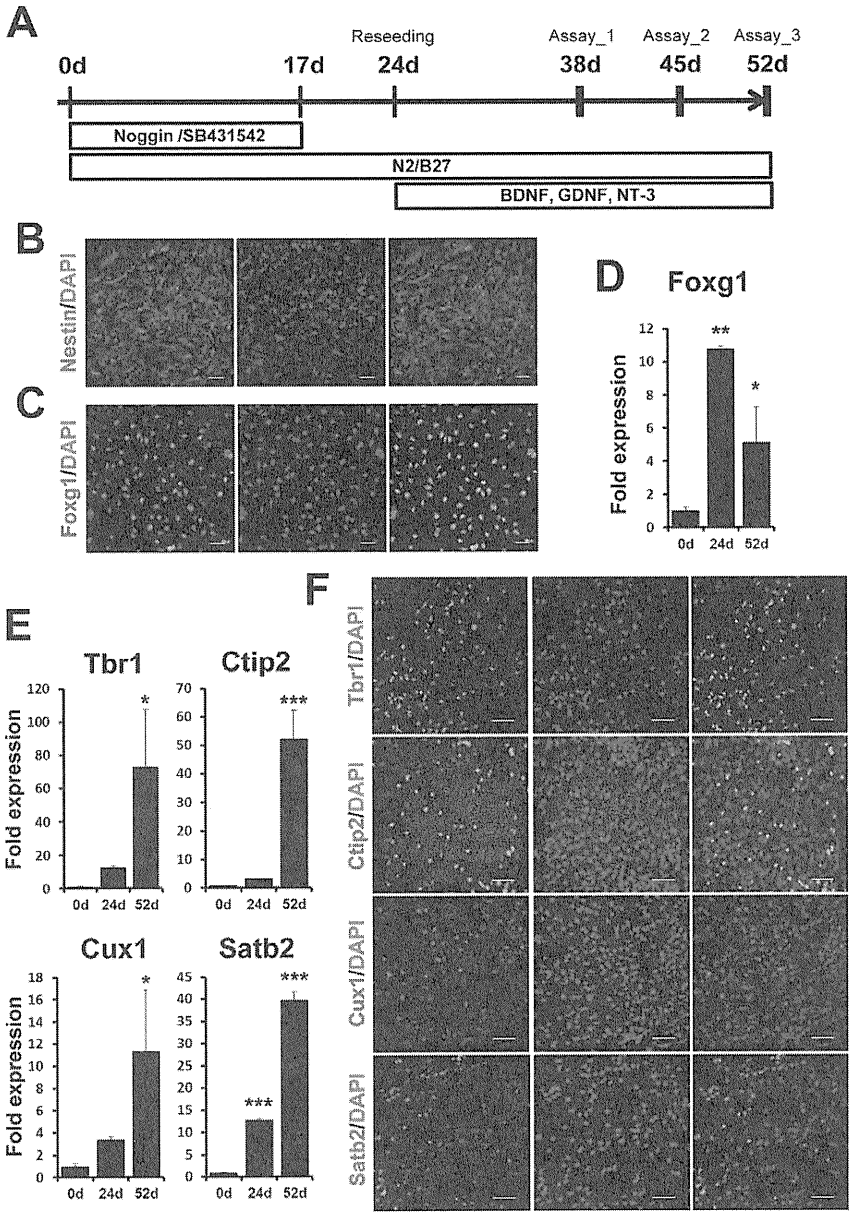

Figure 1. Differentiation of forebrain neurons from hiPS cells. (A) Experimental scheme of neural differentiation from hiPS cells, 253G4. Nestin-positive neuroepithelial cells (B) and Foxg1-positive cells (C) were observed at days 17 and 24, respectively. Scale bar, 50 μm. Expression levels of Foxg1 (D) and the neocortical markers Tbr1, Ctip2, Cux1, and Satb2 (E) at days 0, 24, and 52. Expression levels were measured by qPCR and normalized by that of GAPDH. "Fold expression" is shown as a ratio of day 24/day 0 or day52/day 0. Each column represents the mean ± SD of 3 assays. $^{*}p<0.05$, $^{**}p<0.01$, $^{***}p<0.001$, significantly different from day 0 by Dunnett's test. (F) ICC staining of Tbr1-, Ctip2-, Cux1- and Satb2-positive cells at day 52. Scale bar, 50 μm.
doi:10.1371/journal.pone.0025788.g001

western blotting, but their expression levels did not change markedly over time (Figure 4A, C). Aph-1 has two isoforms in human, Aph-1A and Aph-1B, which are considered to have different effects on the production of Aβ species related to AD [24]. Their expression levels measured by qPCR were relatively constant (Figure 4D). The Aph-1B/Aph-1A ratios also did not show significant differences among the time points analyzed here (Figure 4E).

Aβ has several species, including Aβ40 and Aβ42, which have emerged as two of the most robust Aβ measurements in brain. Recent studies suggest that Aβ40 and Aβ42 may have different effects on Aβ aggregation or oligomerization [25,26]. We measured Aβ40 and Aβ42 secreted into conditioned media for 2 days by sandwich ELISA. Both types of Aβ increased with time (Figure 5A). The level of Aβ40 was higher than that of Aβ42, compatible with previous reports [4,27,28,29,30]. Interestingly, the ratio of Aβ42/Aβ40 was highest at day 38, and there was no significant difference between days 45 and 52 (Figure 5B).

Inhibition of Aβ40 and Aβ42 secretion

We examined whether the differentiated neurons contained funtional β- and γ-secretases and whether Aβ secretion could be controlled. We selected the most effective, commercially available β- and γ-secretase inhibitors, β-secretase inhibitor IV (BSI) [31]

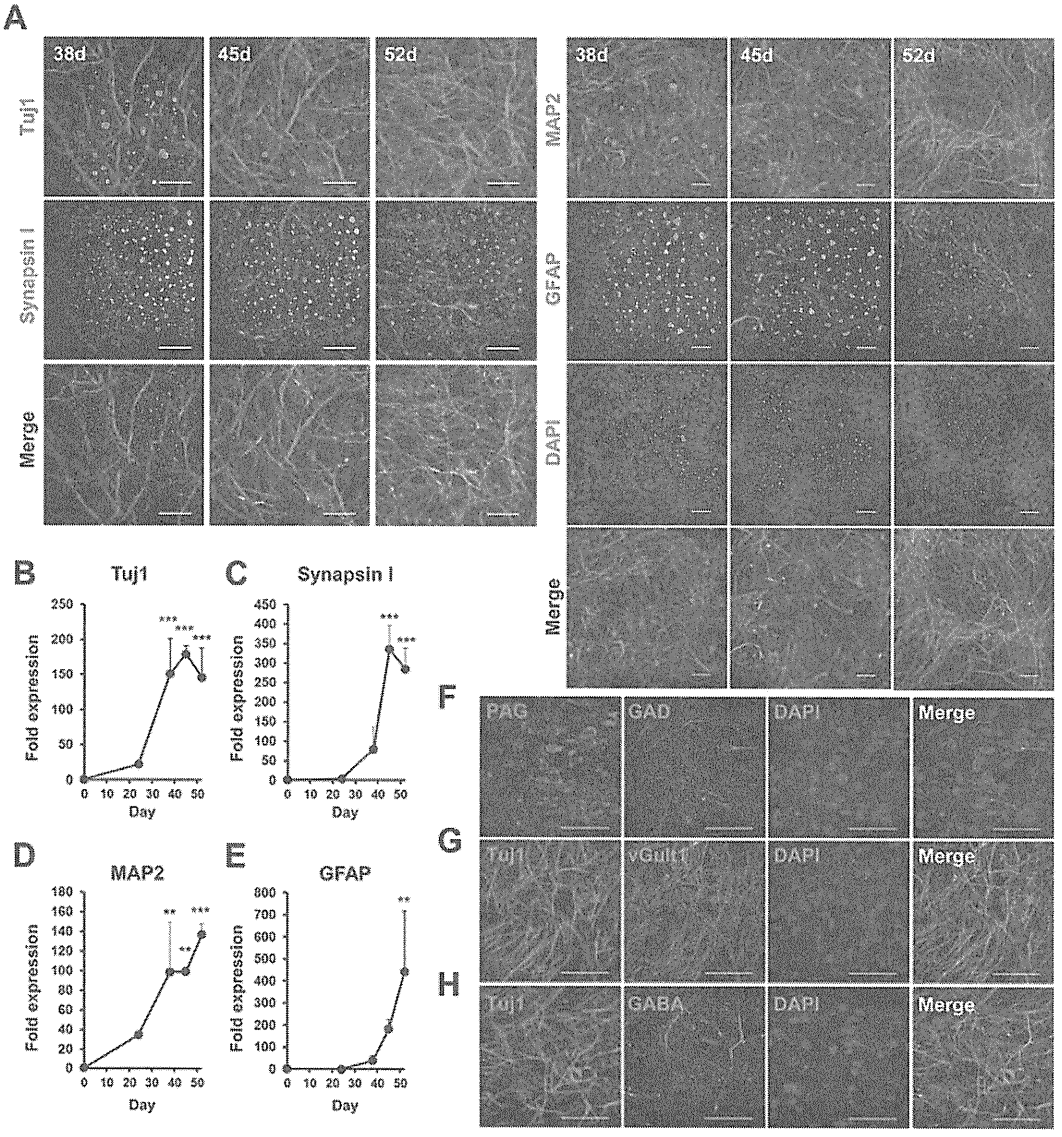

Figure 2. Characterization of neuronal and glial cells differentiated from hiPS cells. (A) Time-dependent morphological changes of cells reseeded in a 24-well plate. Neuronal and glial cells were stained by anti-Tuj1 (left; red), anti-synapsin I (left; green), anti-MAP2 (right; red), and anti-GFAP (right; green) antibodies and DAPI (right; blue) at 38, 45, and 52 days. Scale bar, left; 20 μm, right; 50 μm. Expression levels of Tuj1 (B), synapsin I (C), MAP2 (D), and GFAP (E) at days 0, 24, 38, 45, and 52 were measured by qPCR and normalized by that of GAPDH. "Fold expression" is the ratio of expression at each day compared to day 0. Each point represents mean ± SD of 3 assays. $^{*}p<0.05$, $^{**}p<0.01$, $^{***}p<0.001$, significantly different from day 0 by Dunnett's test. (F–H) Neurotransmitter phenotypes at day 52. PAG (red)- and GAD (green)-positive (F), vGlut1 (green)- and Tuj1 (red)-positive (G), and GABA (green)- and Tuj1 (red)-positive cells (H). Blue, DAPI. Scale bar, 50 μm.
doi:10.1371/journal.pone.0025788.g002

and γ-secretase inhibitor XXI/Compound E (GSI) [32], respectively. We also examined the effect of a non-steroidal anti-inflammatory drug (NSAID), sulindac sulfide [33], because some NSAIDs directly modulate γ-secretase activity to selectively lower Aβ42 levels [33,34]. The cells were treated with each drug for 2 days, and Aβ was monitored in the collected media at day 38 or 52.

There were different susceptibilities to all three drugs between days 38 and 52 (Figure 6) as revealed by two-way analysis of variance (ANOVA) [significant interaction between day and dose (BSI, $p<0.001$ in Aβ40 and Aβ42, respectively; GSI, $p<0.001$ in Aβ40 and Aβ42, respectively; NSAID, $p<0.001$ in Aβ42)]. Following BSI and NSAID treatment, secretion of Aβ40 and Aβ42 was decreased in a dose-dependent manner (Figure 6A, B, E, and F). NSAID especially showed more efficient inhibition of Aβ42 than that of Aβ40, consistent with a previous report [33]. Following GSI treatment (Figure 6C, D), secretion of both Aβ40 and Aβ42 was increased at lower doses (10^{-11}–10^{-8} M), but was inhibited at higher doses (10^{-7}–10^{-6} M) at day 52. This phenomenon, which is called a "gradual Aβ rise", was observed following the addition of other GSIs in a cell line system [35]. On the other hand, secretion of both Aβ40 and Aβ42 at day 38 showed a fast increase at lower doses (10^{-11}–10^{-9} M) (Aβ surge) and drastic decline at 10^{-8} M. We also examined the effects of these inhibitors on cell viability using the lactate dehydrogenase (LDH) assay. Two-day-treatments with the highest concentrations

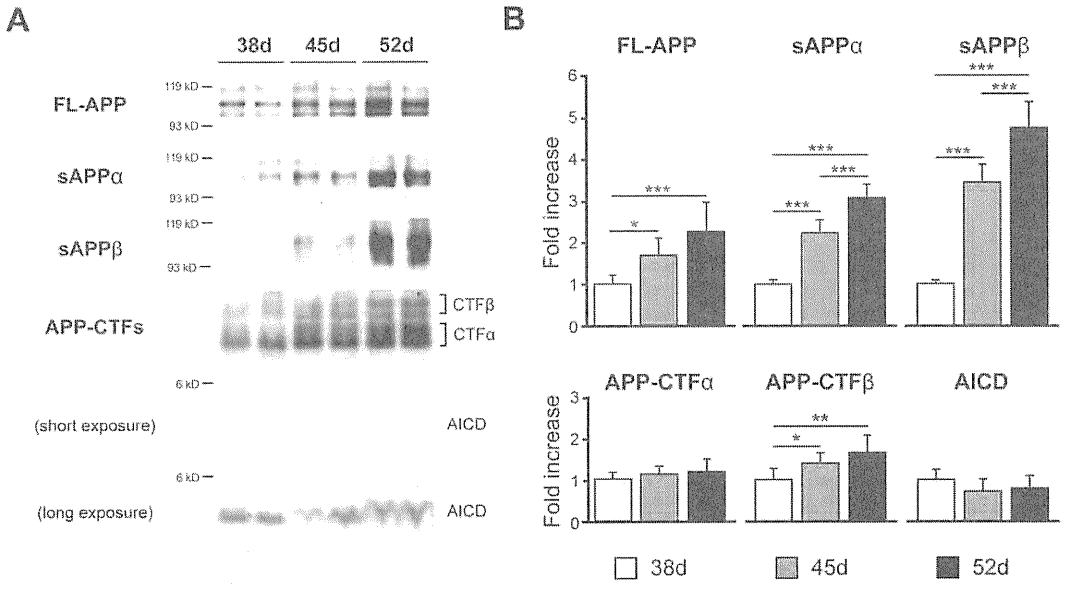

Figure 3. APP was expressed in hiPS cell-derived neuronal cells. HiPS cell-derived neuronal cells express full-length APP, sAPPα, sAPPβ, APP-CTFα, APP-CTFβ and AICD at 38, 45, and 52 days. (A) Representative western blots of APP and its fragments. (B) Each column represents mean ± SD of 8 samples measured by quantitative western blot analysis and normalized by that of β-actin. "Fold expression" represents the ratio of expression on the given day compared to day 38. $^{*}p<0.05$, $^{**}p<0.01$, $^{***}p<0.001$, Tukey's test.
doi:10.1371/journal.pone.0025788.g003

of BSI, GSI, or NSAID did not induce cell death (Table S1). We also traced these experiments using human ES (hES) cell (H9)-derived neuronal cells (Figure S4) because remaining expression of reprogramming factors, Oct3/4 and Klf4, were observed in hiPS cell (253G4)-derived neuronal cells (Figure S6). The Aβ production and its inhibition by these drugs in hES cell-derived neuronal cells were relatively similar to those in hiPS cell-derived ones (Figure S5). These data showed that BSI, GSI, and NSAID partially or fully blocked Aβ production in the hiPS cell-derived neuronal cells, indicating that these cells expressed functional β- and γ-secretases.

Discussion

AD is the most common cause of dementia in the elderly, with progressive neuronal loss in the cerebral cortex and hippocampal formation. Although the underlying etiology of most AD remains unclear, Aβ is thought to play a pivotal role in its pathogenesis. Studies from animal and cellular models have shown that mutations in the APP, PS1, and PS2 genes affected the production of Aβ, which contributes to the formation of amyloid plaques [19]. In several strains of mouse models, Aβ levels in brain tissue, cerebrospinal fluid (CSF), and plasma have been associated with AD pathogenesis and cognitive impairment [27,28,36]. Human samples from clinical AD patients have also been used for pathological and biochemical analyses to understand the etiology of AD. Aβ levels in CSF and plasma have been examined to evaluate their risks for AD [29,37], but brain tissues are only available postmortem for such analyses. On the other hand, immortalized human cell lines derived from kidney or brain, primary neurons derived from mice and rats, or cells artificially overexpressing APP or presenilin with or without familial AD mutations have been utilized for *in vitro* studies [4,30]. There is no doubt that these cells are quite different from living neurons in the human body in terms of innate qualities. Although we have had no choice until recently, important advances in technology of iPS cells may now provide the opportunity to use intact human-derived neuronal cells [38].

We evaluated whether iPS cell-derived neuronal cells could be applied to an *in vitro* cell-based assay system for AD research. In particular, further investigations into the metabolic mechanisms of Aβ are requisite for drug development to treat the brains of patients afflicted with AD. In this respect, we provide a profile of the molecular components associated with Aβ production in hiPS cell-derived neuronal cells and propose to add an Aβ assay system using these cells to the panel of generalized Aβ-monitoring systems (Table 1). Human neuronal cells are considered to provide more accurate human neuronal conditions within which to evaluate drug efficacy or toxicity than other human cell lines (e.g., cancer lines). Furthermore, we would be able to investigate how hiPS cell-derived neuronal cells reflect AD-related physiological and pathological conditions based on Aβ production.

In the present study, we characterized iPS cell-derived neuronal cells in terms of their expression of neuronal and glial markers by exposing them to Noggin and SB431542 during their differentiation (Figures 1 and 2). We observed increases in GFAP mRNA levels and in synapsin I-positive synaptic puncta at day 52. This was consistent with data showing that the existence of astrocytes promotes synaptic activity in human ES cell-derived neurons [40]. When differentiation occurred in the presence of non-morphogens, we obtained mainly glutamatergic neurons (Figure 2F, G), quite in line with previous reports of concerning hES and hiPS cells [10,11]. Expression of the forebrain marker Foxg1 suggests a default forebrain identity of the 253G4 iPS cells used in this study (Figure 1C, D). We also observed the expression of the neocortex-specific transcriptional factors Tbr1, Ctip2, Cux1, and Satb2 (Figure 1E, F). These expression schemes appear to mimic human neocortical development *in vitro* [16], although further analyses are needed to assist in understanding human neuronal subtype-specific differentiation.

This is the first study to observe the expression of APP, β- and γ-secretase, and the production of Aβ in hiPS cell-derived neuronal

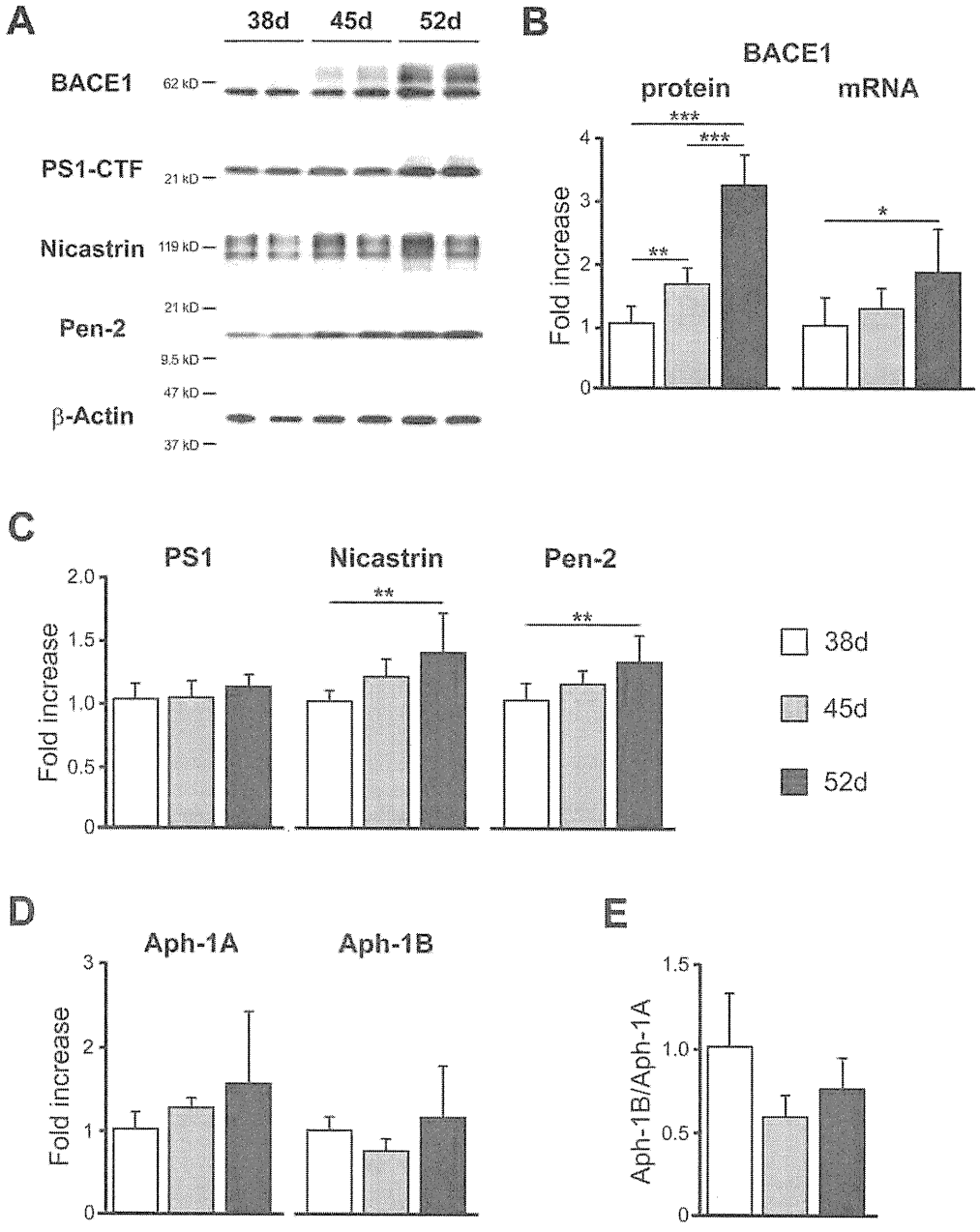

Figure 4. β-Secretase and γ-secretase components were expressed in hiPS cell-derived neuronal cells. The hiPS cell-derived neuronal cells express BACE1 protein and mRNA (B), γ-secretase components; presenilin 1(PS1), nicastrin, Pen-2 (C), and Aph-1A, and Aph-1B (D) at days 38, 45, and 52. Expression levels were quantified by western blot analysis (n = 8) (B, C) or qPCR (n = 3) (D) and normalized by that of β-actin. "Fold expression" represents the ratio of expression on the given day compared to day 38. (E) The ratio Aph-1B/Aph-1A. Data represent mean ± SD. (A) Representative western blots of BACE1 and γ-secretase components at 38, 45, and 52 days. $^{*}p<0.05$, $^{**}p<0.01$, $^{***}p<0.001$, Tukey's test.
doi:10.1371/journal.pone.0025788.g004

cells. APP, sAPPβ, APP-CTFβ and BACE1 protein levels were increased (Figures 3 and 4), but protein levels of γ-secretase components were not significantly different during the period from day 38 to 52 (Figure 4C, D). Aβ production in hiPS cell 253G4-derived neuronal cells increased with differentiation course (Figure 5A), however that in another hiPS cell 201B7 [5]- and in hES H9-derived neuronal cells did not increase (Figures S5 and S7) although all cell lines showed development of synapse (Figure S4A) as Aβ releasing site [41], indicating that besides synaptogenesis, subtle changes in localization and assembly of APP [42], BACE1, γ-secretase components would be critical for Aβ production.

The Aβ42/Aβ40 ratio unexpectedly showed a significant decrease from day 38 to 45 (Figure 5B). Serneels *et al.* reported that the γ-secretase complex containing Aph-1B was active and involved in the generation of amyloidogenic Aβ42 [24]. Our data showed that the Aph-1B/Aph-1A ratio did not change significantly with cell differentiation (Figure 4E); therefore, the Aβ42/Aβ40 ratio may be influenced by other unknown factors interacting directly or indirectly with γ-secretase.

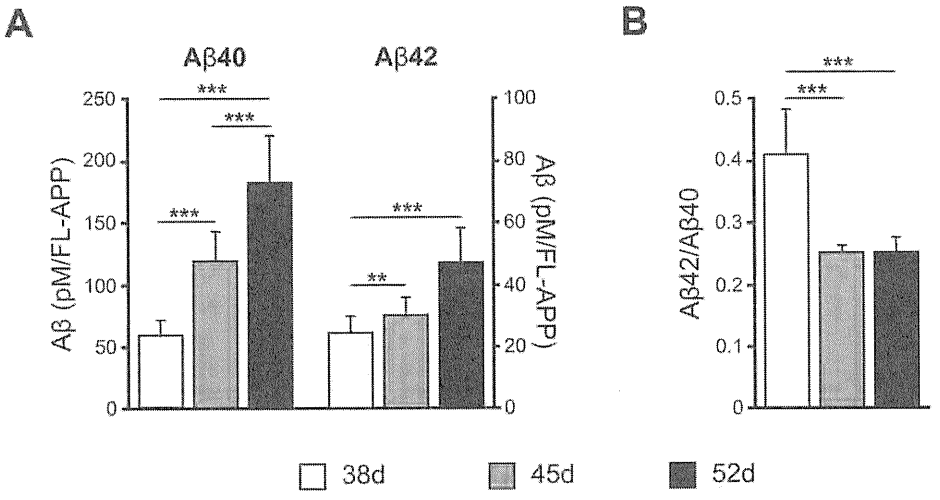

Figure 5. Aβ was produced in hiPS cell-derived neuronal cells. (A) Aβ40 or Aβ42 secreted into the conditioned media and FL-APP were measured by sandwich ELISA and western blot analysis, respectively. Expression level of Aβ was normalized by that of FL-APP. (B) Aβ42/Aβ40 ratios. Data represent the mean ± SD of 8 assays. $^{*,\#}p<0.05$, $^{**,\#\#}p<0.01$, $^{***,\#\#\#}p<0.001$, Tukey's test.
doi:10.1371/journal.pone.0025788.g005

BSI, GSI, and the NSAID sulindac sulfide inhibited Aβ production in this human neuronal cell system (Figure 6). The inhibitory effect on Aβ production by GSI showed a characteristic difference between days 38 (Aβ surge) and 52 (gradual Aβ rise) (Figure 6C, D). Aβ surge at day 38 was also observed in another hiPS cell (201B7)-derived neuronal cells (Figure S7) as well as in hES cell line, H9-derived ones (Figure S5). At day 38, GSI might promote neuronal differentiation with synaptogenesis via blocking Notch signaling [43] rather than inhibition of Aβ production, leading to Aβ surge. Another possible explanation for Aβ surge is that change in conformation or components of the γ-secretase affects the sensitivity of γ-secretase to GSI (total Aβ, Aβ40, Aβ42, and Aβ42/Aβ40), although levels of mRNA and the ration for Aph-1A and Aph-1B do not change between days 38 and 52 (Figure 4D, E) Thus, for precise Aβ monitoring in human stem cell-derived neuronal cells, it is necessary to use neuronal cells with a sufficient substrate level and synaptogenesis, because Aβ is released presynaptically, as mentioned above.

Some NSAIDs are known to preferentially lower Aβ42 [33,34]. Our data showed that sulindac sulfide was capable of inhibiting Aβ42 secretion at high concentrations ($\geq 10^{-5}$ M) (Figure 6F), although a few NSAIDs do not show therapeutic effects for AD. Negative results might be due to low γ-secretase modulator potency [44]. To discover novel effective drugs for modulating β- or γ-secretase activity, the *in vitro* hiPS cell-derived neuronal cell assay system might be expected to yield such drugs.

Familial AD patient specific neuronal cells generated by direct conversion (induced neuron, iN) show higher Aβ42/Aβ40 ratio than those of unaffected individuals [45]. Based on this report, hiPS/hES cell-derived neurons expressing mutant PS1, PS2, or APP may show higher Aβ42/Aβ40 ratio. Comparing to our results, the levels of Aβs in this assay (Aβ40; ~1.7 ng/ml at day 52) is higher than that using iN cells (Aβ40; ~0.1 ng/ml), although iN cells become functional neurons more quickly. The optimization of neuronal cell condition for comparison of the Aβ42/Aβ40 ratio between multiple iPS cell-derived neuronal cells may be required.

In conclusion, our findings indicate that hiPS cell-derived neuronal cells express functional β- and γ-secretases related to the production of Aβ in the present experimental conditions. In addition, our data provide the proof in principle that hiPS cell-derived neuronal cells can be applied to drug screening and AD patient-specific iPS cell research.

Materials and Methods

Antibodies and reagents

Primary antibodies used were as follows: mouse anti-Nestin (1:200, Millipore, Temecula, CA), mouse anti-Tuj1 (1:2000, Covance, Princeton, NJ), rabbit anti-GFAP (1:500, DAKO, Carpinteria, CA), rabbit anti-Synapsin I (1:500, Millipore), mouse anti-Cux1 (1:100, Abnova, Taipei, Taiwan), rabbit anti-Satb2 (1:1000, Abcam, Cambridge, UK), rat anti-Ctip2 (1:500, Abcam), rabbit anti-Tbr1 (1:500, Abcam), rabbit anti-vGlut1 (1:1000, Synaptic Systems, Göttingen, Germany), rabbit anti-Foxg1 (1:100, Abcam), rabbit anti-GABA (1:1000, Sigma-Aldrich, St. Louis, MO), rabbit anti-GAD65/67 (1:200, Millipore), mouse anti-PAG [46] (1:500), rabbit anti-APP (1:15000, Sigma-Aldrich), mouse anti-APP (1 μg/ml, Millipore), rabbit-anti BACE (1:2000, Merck, Darmstadt, Germany) mouse anti-PS1 loop C-terminus (1:1000, Millipore), rabbit anti-nicastrin (1 μg/ml, Thermo Scientific, Rockford, IL), rabbit anti-Pen-2 (1:1000, Invitrogen, San Diego, CA), mouse anti-MAP2 (1:200, Millipore), goat anti-ChAT (1:100, Millipore), guinea pig anti-VAChT (1:500, Millipore), and mouse anti-β-actin (1:15000, Sigma-Aldrich). We raised rabbit polyclonal antibodies against the carboxyl terminals of human sAPPα (hsAPPα) and sAPPβ using the KLH-conjugated synthetic peptides CRHDSGYEVHHQK and CKTEEISEVKM, respectively (Figure S3). All animal experiments were performed in compliance with the institutional guidelines at RIKEN Brain Science Institute, and were approved by the Animal Care and Use Committee (Permit number: H17-2B031). Each antibody was purified with a peptide-conjugated column [47]. Alexa Fluor 488 and Alexa Fluor 594-conjugated secondary antibodies (Invitrogen) were used for immunofluorescence.

The β-secretase inhibitor IV [31] and γ-secretase inhibitor XXI/Compound E [32] were purchased from Merck. Sulindac sulfide (NSAID) was purchased from Sigma-Aldrich.

Immunocytochemistry

Cells were fixed with 4% paraformaldehyde in phosphate buffered saline (PBS) for 30 min, and incubated in PBS

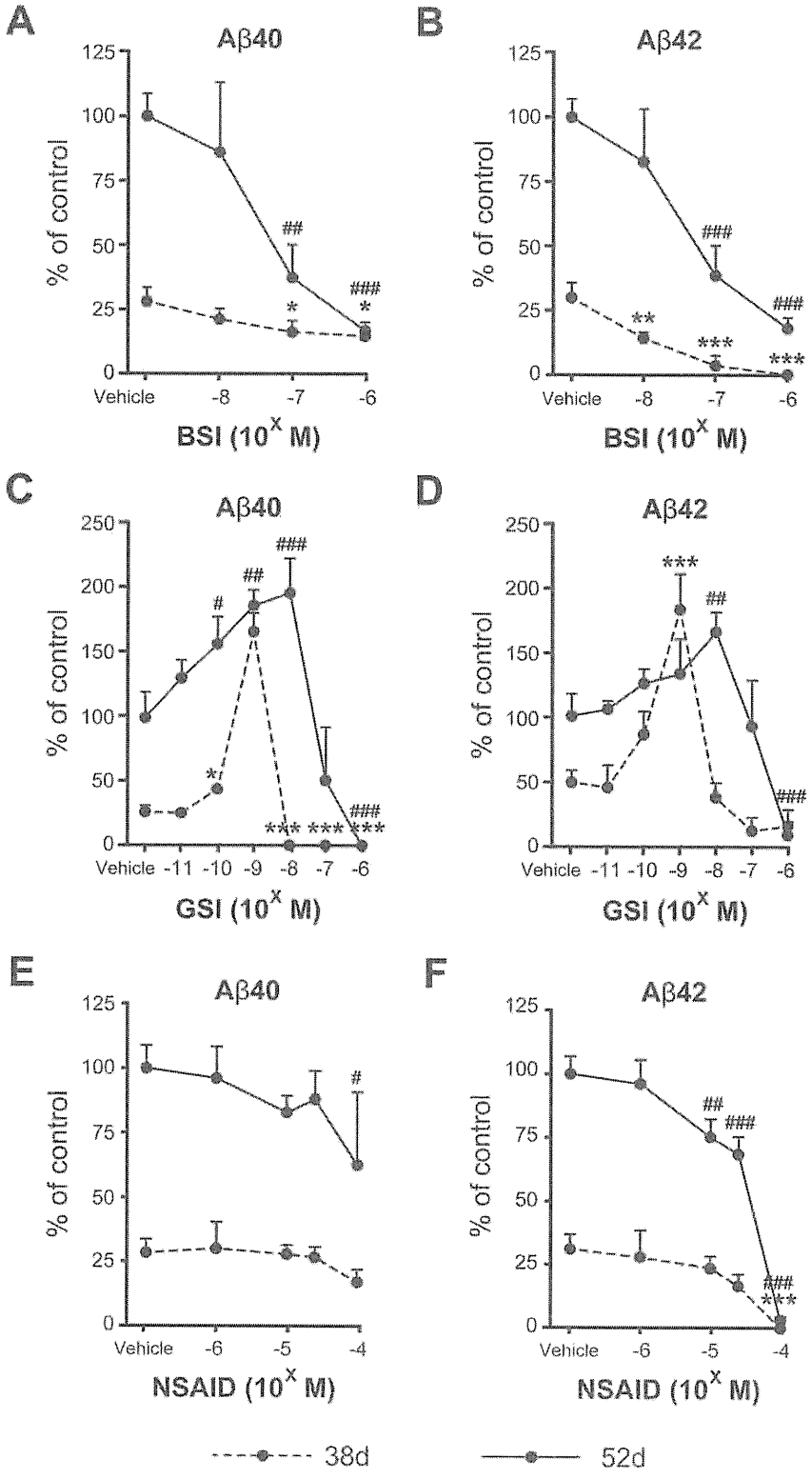

Figure 6. Aβ production was modulated by β- and γ-secretase inhibitors and an NSAID. β-Secretase inhibitor (BSI) (A, B), γ-secretase inhibitor (GSI) (C, D), and NSAID (E, F) were added into hiPS cell-derived neuronal cell cultures at day 36 (dotted line) and 50 (bold line), and two days later amounts of Aβ40 and Aβ42 secreted into the conditioned media were measured. The ratios Aβ40/FL-APP and Aβ42/FL-APP are expressed as percentages of the vehicle-treated group at day 52 and represent mean ± SD of 3 assays. A, B: There were significant main effects of day ($F(1, 16) = 72.5$ and 162.4, $p<0.001$ in Aβ40 and Aβ42, respectively) and dose ($F(3, 16) = 23.1$ and 45.7, $p<0.001$ in Aβ40 and Aβ42, respectively), and significant interaction between day and dose ($F(3, 16) = 13.0$ and 11.7, $p<0.001$ in Aβ40 and Aβ42, respectively) by 2-way ANOVA. C, D: There were significant main effects of day ($F(1, 28) = 240.5$ and 59.1, $p<0.001$ in Aβ40 and Aβ42, respectively) and dose ($F(6, 28) = 70.8$ and 37.8, $p<0.001$ in Aβ40 and Aβ42, respectively), and significant interaction between day and dose ($F(6, 28) = 23.5$ and 15.1, $p<0.001$ in Aβ40 and Aβ42, respectively) by

2-way ANOVA. E, F: There were significant main effects of day ($F(1, 20) = 196.9$ and 418.0, $p<0.001$ in Aβ40 and Aβ42, respectively) and dose ($F(4, 20) = 4.16$, $p = 0.013$ and $F(4, 20) = 91.9$, $p<0.001$ in Aβ40 and Aβ42, respectively), and significant interaction between day and dose ($F(4, 20) = 25.4$, $p<0.001$ in Aβ42) by 2-way ANOVA. $^{*}, ^{\#}p<0.05$, $^{**}, ^{\#\#}p<0.01$, $^{***}, ^{\#\#\#}p<0.001$, significantly different from respective vehicle-treated groups by Dunnett's test.
doi:10.1371/journal.pone.0025788.g006

containing 0.2% Triton X-100 for 10 min (permeabilization). After blocking with 2% BSA in PBS, cells were incubated with primary antibody diluted with blocking buffer and then washed with PBS. Finally the cells were incubated with secondary antibodies and mounted using ProLong Gold antifade reagent with DAPI (Invitrogen). The immunoreactive cells were visualized using an LSM 700 Laser Scanning Microscope (Carl Zeiss, Jena, Germany) and a Biorevo BZ-9000 fluorescence microscope (Keyence, Osaka, Japan).

Quantitative real-time RT-PCR

Total RNA was isolated from cells using TRIZOL reagent (Invitrogen). Contaminating DNA was removed using the TURBO DNA-free kit (Ambion, Austin, TX), and cDNA was synthesized using ReverTra Ace-α (Toyobo, Osaka, Japan), according to the manufacturers' protocols. Real-time PCR was performed using the StepOnePlus system (Applied Biosystems) and SYBR green reagent (TAKARA, Shiga, Japan). The primers used are listed in Table S2 in the supporting information.

HiPS cell culture and differentiation into neuronal cells

HiPS cells, 253G4 [14] (passage 20–30) or hES cells, H9 were cultured on mitomycin C-treated mouse embryonic fibroblasts in primate ES medium (ReproCELL, Kanagawa, Japan) supplemented with bFGF (Wako Pure Chemicals, Osaka, Japan). To obtain cortical neurons derived from iPS cells, we partially modified a previous method [12,15]. For neural induction, partially dissociated iPS cell colonies, 40–100 μm in diameter, were selected with Cell Strainer (BD Falcon, BD Bioscience, Bedford, MA) and plated on poly-L-lysine (Sigma-Aldrich)/Laminin (BD Biosciences) (PLL/LM)-coated dishes (P1) in N2B27 neuronal differentiation medium [DMEM/F12 (Invitrogen), Neurobasal (Invitrogen), N2 (Invitrogen), B27 minus vitamin A (Invitrogen), L-Gln (Invitrogen)], supplemented with 100 ng/ml human recombinant Noggin (R&D Systems, Minneapolis, MN) and 1 μM SB431542 (Sigma-Aldrich) for 17 days. At day 10, primary colonies were split into small clumps using 200 U/ml collagenase with $CaCl_2$ and plated into PLL/Entactin-Collagen IV-Laminin (Millipore) (ECL)-coated dishes (P2). At day 17, P2 cells were dissociated using Accutase (Innovative Cell Technologies, San Diego, CA) and cultured on PLL/ECL-coated dishes (P3). Finally, at day 24, cells dissociated with Accutase were passed through a 40-μm cell strainer (BD Biosciences), counted, and cultured on PLL/LM/Fibronectin (Millipore)-coated 24-well plates at 2.5×10^4 cells/well in N2B27 medium supplemented with 10 ng/ml BDNF, GDNF, and NT-3 (R&D Systems). Medium changes for cell culture were carried out once every two or three days until day 52.

Aβ sandwich ELISA

At days 38, 45, and 52, two-day incubated conditioned media were collected from cultured neuronal cells and centrifuged at 4,000 *g* for 10 min. The resultant clear supernatants were subjected to sandwich ELISA (Wako) with a combination of monoclonal antibodies specific to the midportion of Aβ and specific to the C-terminal of Aβ40 or Aβ42, to determine the amounts of secreted Aβ, as described previously [20,28,30]. We also examined the inhibitory effect of each drug on Aβ production. All media were replaced with new media containing each drug and two-day conditioned media were analyzed as mentioned above.

Western blot analysis

Western blot analysis was performed as previously described with minor modification. In addition to conditioned media, cell lysates were also collected, extensively washed with PBS, and lysed

Table 1. Panel of Aβ monitoring systems.

Human sample	**Aβ40**	**Aβ42**	**Ref.**
Brain tissue [AD]	↑ (AD/NC)	↑ (AD/NC)	[39]
CSF [AD]	-	↓ (AD/NC)	[37]
	→ (AD/NC)	↓ (AD/NC)	[29]
Plasma [AD]	↑ (AD/NC)	→ (AD/NC)	[29]
iPS cell-derived neuronal cells	Measurable	Measurable	This report
Mouse model	**Aβ40**	**Aβ42**	**Ref.**
Brain [PDAPP]	↑ (Aging)	↑ (Aging)	[36]
Brain [APP23]	↑ (Tg/non-Tg)	↑ (Tg/non-Tg)	[27]
Brain [Tg2576]	↑ (Aging)	↑ (Aging)	[28]
	↑ (Tg/non-Tg)	↑ (Tg/non-Tg)	
CSF [Tg2576]	↓ (Aging)	↓ (Aging)	[28]
Plasma [Tg2576]	↓ (Aging)	↓ (Aging)	[28]
Cell line	**Aβ40**	**Aβ42**	**Ref.**
[APP_{NL}-H4]	Measurable	Measurable	[30]
[CHO-APP_{NL}/SH-SY5Y-APP]	Measurable	Measurable	[4]

AD, Alzheimer's disease; NC, normal control; Tg, transgenic mouse model.
doi:10.1371/journal.pone.0025788.t001

directly with 1× sample buffer (EzApply; ATTO, Tokyo, Japan). The media or cell lysates were separated by 5–20% gradient or 7.5% [FL-APP] or 10% [β-actin] sodium dodecyl sulfate-polyacrylamide gel electrophoresis (SDS-PAGE) and transferred to polyvinylidene difluoride membranes (Hybond-P; GE Healthcare, Buckinghamshire, UK). The blots were probed with an appropriate primary antibody, followed by HRP-conjugated anti-mouse or anti-rabbit IgG (GE Healthcare). The protein bands were visualized using an enhanced chemiluminescence (ECL) detection method (GE Healthcare), and band intensity was analyzed with a densitometer (LAS-4000; GE Healthcare), using the Science Laboratory 2001 Image Gauge software (Fujifilm, Tokyo, Japan). Immunoreactive protein content in each sample was calculated based on a standard curve constructed with each recombinant protein or one of the samples. Each set of experiments was repeated at least two times to confirm the results. The level of β-actin protein, measured by quantitative western blotting using β-actin antibody, was used as an extraction and loading control.

LDH assay

Cell toxicity assays were performed using a cytotoxicity detection kit (LDH, Roche, Mannheim, Germany) according to the manufacturer's protocol.

Statistical analysis

All data were expressed as mean ± SD. Comparisons of mean among more than three groups were done by one-way or two-way ANOVA, followed by *post-hoc* test (PRISM, GraphPad software). *P* values ≤0.05 indicated significant differences.

Supporting Information

Figure S1 Cholinergic neuronal marker-positive cells were observed in hiPS cell-derived neuronal cells. Expression levels of ChAT (A) and VAChT (B) were quantified by qPCR (n = 3) and normalized by that of GAPDH. "Fold expression" represents the ratio of expression on the given day compared to day 38. ChAT- (C) and VAChT (D)-positive cells were observed a little at day 52.
(TIF)

Figure S2 Percentages of the three isoforms of APP (APP770, APP751, and APP695) at 38, 45, and 52 days. Each column represents mean ± SD of 8 assays. $^{*}p<0.05$, $^{**}p<0.01$, $^{***}p<0.001$, Tukey's test.
(TIF)

Figure S3 New hsAPPα and sAPPβ antibodies specifically detect human sAPPα and sAPPβ by western blots, respectively. Human neuroglioma H4 cells overexpressing wild-type APP (APP_{WT}-H4 cells) were treated with α-secretase activator (12-*O*-tetradecanoylphorbol 13-acetate (TPA)), α-secretase inhibitor (TNF-α protease inhibitor-2 (TAPI-2)), or β-secretase inhibitor (see Protocol S1). Brain lysates of APP-knockout mice (APP-KO) were used as negative control. Immunoblots of conditioned media and supernatants of brain lysates were probed by anti-hsAPPα or anti-sAPPβ antibody. sAPPα or sAPPβ derived from both exogenous APP695 and endogenous APP770/751 are detected by each antibody. The increase in sAPPα by α-secretase activator and the reduction in sAPPα by α-secretase inhibitor effectively reached 434% and 50% of control (DMSO), respectively (upper panel). The decrease in sAPPβ by β-secretase inhibitor effectively reached 11% of control (lower panel). Neither sAPPα nor sAPPβ in the APP-KO brain was detected by anti-hsAPPα or anti-sAPPβ antibody, respectively. An asterisk indicates a non-specific band.
(TIF)

Figure S4 Immunocytochemical characterization of human ES cell (H9)-derived neuronal cells. (A) Time-dependent morphological changes of cells reseeded in a 24-well plate. Neuronal and glial cells were stained by anti-Tuj1 (left; red), anti-synapsin I (left; green), anti-MAP2 (right; red), and anti-GFAP (right; green) antibodies and DAPI (right; blue) at 38, 45, and 52 days. Scale bar, left; 20 μm, right; 50 μm. (B) ICC staining of Tbr1-, Ctip2-, Cux1- and Satb2-positive cells at day 52. (C–E) Neurotransmitter phenotypes at day 52. PAG (red)- and GAD (green)-positive (C), Glut1 (green)- and Tuj1 (red)-positive (D), and GABA (green)- and Tuj1 (red)-positive cells (E). Blue, DAPI. Scale bar, 50 μm.
(TIF)

Figure S5 Aβ production was modulated by several drugs in human ES cell-derived neuronal cells. β-Secretase inhibitor (BSI) (A, B), γ-secretase inhibitor (GSI) (C, D), and NSAID (E, F) were added into hES cell-derived neuronal cell cultures at day 36 (dotted line) and 50 (bold line), and two days later amounts of Aβ40 and Aβ42 secreted into the conditioned media were measured. The ratios Aβ40/FL-APP and Aβ42/FL-APP are expressed as percentages of the vehicle-treated group at day 52 and represent mean ± SD of 3 assays. $^{*,\ \#}p<0.05$, $^{**,\ \#\#}p<0.01$, $^{***,\ \#\#\#}p<0.001$, significantly different from respective vehicle-treated groups by Dunnett's test.
(TIF)

Figure S6 Expression levels of reprogramming factors of iPS cells in neural differentiation. Total and transgene (Tg) expression levels of Sox2, Oct3/4 and Klf4 were measured by qPCR. Bold and dotted lines represent total and transgene expressions, respectively. "Fold expression" represents the ratio of the expression level compared to the total expression level at day 0 (iPS cells).
(TIF)

Figure S7 Aβ production was modulated by GSI in human iPS cell (201B7)-derived neuronal cells. γ-Secretase inhibitor (GSI) was added into the hiPS cell line, 201B7-derived neuronal cell cultures at day 36 (dotted line) and 50 (bold line), and two days later amounts of Aβ40 (A) and Aβ42 (B) secreted into the conditioned media were measured. The ratios Aβ40/FL-APP and Aβ42/FL-APP are expressed as percentages of the vehicle-treated group at day 52 and represent mean ± SD of 3 assays.
(TIF)

Protocol S1 Sampling method for checking antibody specificity.
(PDF)

Table S1 Effects of secretion inhibitors on cell viability measured by LDH assay at day 52.
(DOCX)

Table S2 qPCR primers.
(DOCX)

Acknowledgments

We would like to express our sincere gratitude to all our coworkers and collaborators, especially to K. Watanabe (RIKEN Brain Science Institute & Nagasaki University) for technical assistance and to K. Murai (CiRA) for editing manuscript.

Author Contributions

Conceived and designed the experiments: NI HI NY MA. Performed the experiments: NY MA NI. Analyzed the data: NY MA NI HI. Contributed reagents/materials/analysis tools: SK KT IA HH TK KM TCS TN TA SY. Wrote the paper: NY MA SY NI HI.

References

1. Selkoe DJ (2002) Alzheimer's disease is a synaptic failure. Science 298: 789–791.
2. Iwata N, Higuchi M, Saido TC (2005) Metabolism of amyloid-β peptide and Alzheimer's disease. Pharmacol Ther 108: 129–148.
3. Kukar TL, Ladd TB, Bann MA, Fraering PC, Narlawar R, et al. (2008) Substrate-targeting γ-secretase modulators. Nature 453: 925–929.
4. Kounnas MZ, Danks AM, Cheng S, Tyree C, Ackerman E, et al. (2010) Modulation of γ-secretase reduces β-amyloid deposition in a transgenic mouse model of Alzheimer's disease. Neuron 67: 769–780.
5. Takahashi K, Tanabe K, Ohnuki M, Narita M, Ichisaka T, et al. (2007) Induction of pluripotent stem cells from adult human fibroblasts by defined factors. Cell 131: 861–872.
6. Yu J, Vodyanik MA, Smuga-Otto K, Antosiewicz-Bourget J, Frane JL, et al. (2007) Induced pluripotent stem cell lines derived from human somatic cells. Science 318: 1917–1920.
7. Watanabe K, Kamiya D, Nishiyama A, Katayama T, Nozaki S, et al. (2005) Directed differentiation of telencephalic precursors from embryonic stem cells. Nat Neurosci 8: 288–296.
8. Gaspard N, Bouschet T, Hourez R, Dimidschstein J, Naeije G, et al. (2008) An intrinsic mechanism of corticogenesis from embryonic stem cells. Nature 455: 351–357.
9. Eiraku M, Watanabe K, Matsuo-Takasaki M, Kawada M, Yonemura S, et al. (2008) Self-organized formation of polarized cortical tissues from ESCs and its active manipulation by extrinsic signals. Cell Stem Cell 3: 519–532.
10. Li XJ, Zhang X, Johnson MA, Wang ZB, Lavaute T, et al. (2009) Coordination of sonic hedgehog and Wnt signaling determines ventral and dorsal telencephalic neuron types from human embryonic stem cells. Development 136: 4055–4063.
11. Zeng H, Guo M, Martins-Taylor K, Wang X, Zhang Z, et al. (2010) Specification of region-specific neurons including forebrain glutamatergic neurons from human induced pluripotent stem cells. PLoS One 5: e11853.
12. Chambers SM, Fasano CA, Papapetrou EP, Tomishima M, Sadelain M, et al. (2009) Highly efficient neural conversion of human ES and iPS cells by dual inhibition of SMAD signaling. Nat Biotechnol 27: 275–280.
13. Braak H, Braak E (1991) Neuropathological stageing of Alzheimer-related changes. Acta Neuropathol 82: 239–259.
14. Nakagawa M, Koyanagi M, Tanabe K, Takahashi K, Ichisaka T, et al. (2008) Generation of induced pluripotent stem cells without Myc from mouse and human fibroblasts. Nat Biotechnol 26: 101–106.
15. Wada T, Honda M, Minami I, Tooi N, Amagai Y, et al. (2009) Highly efficient differentiation and enrichment of spinal motor neurons derived from human and monkey embryonic stem cells. PLoS One 4: e6722.
16. Saito T, Hanai S, Takashima S, Nakagawa E, Okazaki S, et al. (2011) Neocortical layer formation of human developing brains and lissencephalies: consideration of layer-specific marker expression. Cereb Cortex 21: 588–596.
17. Kim JE, O'Sullivan ML, Sanchez CA, Hwang M, Israel MA, et al. (2011) Investigating synapse formation and function using human pluripotent stem cell-derived neurons. Proc Natl Acad Sci U S A 108: 3005–3010.
18. Akiyama H, Kaneko T, Mizuno N, McGeer PL (1990) Distribution of phosphate-activated glutaminase in the human cerebral cortex. J Comp Neurol 297: 239–252.
19. Blennow K, de Leon MJ, Zetterberg H (2006) Alzheimer's disease. Lancet 368: 387–403.
20. Kitazume S, Tachida Y, Kato M, Yamaguchi Y, Honda T, et al. (2010) Brain endothelial cells produce amyloid β from amyloid precursor protein 770 and preferentially secrete the O-glycosylated form. J Biol Chem 285: 40097–40103.
21. Yang LB, Lindholm K, Yan R, Citron M, Xia W, et al. (2003) Elevated β-secretase expression and enzymatic activity detected in sporadic Alzheimer disease. Nat Med 9: 3–4.
22. O'Connor T, Sadleir KR, Maus E, Velliquette RA, Zhao J, et al. (2008) Phosphorylation of the translation initiation factor eIF2α increases BACE1 levels and promotes amyloidogenesis. Neuron 60: 988–1009.
23. Parks AL, Curtis D (2007) Presenilin diversifies its portfolio. Trends Genet 23: 140–150.
24. Serneels L, Van Biervliet J, Craessaerts K, Dejaegere T, Horré K, et al. (2009) γ-Secretase heterogeneity in the Aph1 subunit: relevance for Alzheimer's disease. Science 324: 639–642.
25. McGowan E, Pickford F, Kim J, Onstead L, Eriksen J, et al. (2005) Aβ42 is essential for parenchymal and vascular amyloid deposition in mice. Neuron 47: 191–199.
26. Ono K, Condron MM, Ho L, Wang J, Zhao W, et al. (2008) Effects of grape seed-derived polyphenols on amyloid β-protein self-assembly and cytotoxicity. J Biol Chem 283: 32176–32187.
27. Hsiao K, Chapman P, Nilsen S, Eckman C, Harigaya Y, et al. (1996) Correlative memory deficits, Aβ elevation, and amyloid plaques in transgenic mice. Science 274: 99–102.
28. Kawarabayashi T, Younkin LH, Saido TC, Shoji M, Ashe KH, et al. (2001) Age-dependent changes in brain, CSF, and plasma amyloid β protein in the Tg2576 transgenic mouse model of Alzheimer's disease. J Neurosci 21: 372–381.
29. Mehta PD, Pirttilä T, Mehta SP, Sersen EA, Aisen PS, et al. (2000) Plasma and cerebrospinal fluid levels of amyloid β proteins 1-40 and 1-42 in Alzheimer disease. Arch Neurol 57: 100–105.
30. Asai M, Iwata N, Tomita T, Iwatsubo T, Ishiura S, et al. (2010) Efficient four-drug cocktail therapy targeting amyloid-β peptide for Alzheimer's disease. J Neurosci Res 88: 3588–3597.
31. Stachel SJ, Coburn CA, Steele TG, Jones KG, Loutzenhiser EF, et al. (2004) Structure-based design of potent and selective cell-permeable inhibitors of human β-secretase (BACE-1). J Med Chem 47: 6447–6450.
32. Seiffert D, Bradley JD, Rominger CM, Rominger DH, Yang F, et al. (2000) Presenilin-1 and -2 are molecular targets for γ-secretase inhibitors. J Biol Chem 275: 34086–34091.
33. Weggen S, Eriksen JL, Das P, Sagi SA, Wang R, et al. (2001) A subset of NSAIDs lower amyloidogenic Aβ42 independently of cyclooxygenase activity. Nature 414: 212–216.
34. Eriksen JL, Sagi SA, Smith TE, Weggen S, Das P, et al. (2003) NSAIDs and enantiomers of flurbiprofen target γ-secretase and lower Aβ 42 in vivo. J Clin Invest 112: 440–449.
35. Burton CR, Meredith JE, Barten DM, Goldstein ME, Krause CM, et al. (2008) The amyloid-β rise and γ-secretase inhibitor potency depend on the level of substrate expression. J Biol Chem 283: 22992–23003.
36. Games D, Adams D, Alessandrini R, Barbour R, Berthelette P, et al. (1995) Alzheimer-type neuropathology in transgenic mice overexpressing V717F β-amyloid precursor protein. Nature 373: 523–527.
37. De Meyer G, Shapiro F, Vanderstichele H, Vanmechelen E, Engelborghs S, et al. (2010) Diagnosis-independent Alzheimer disease biomarker signature in cognitively normal elderly people. Arch Neurol 67: 949–956.
38. Inoue H, Yamanaka S (2011) The use of induced pluripotent stem cells in drug development. Clin Pharmacol Ther 89: 655–661.
39. Iwatsubo T, Saido TC, Mann DM, Lee VM, Trojanowski JQ (1996) Full-length amyloid-β (1-42(43)) and amino-terminally modified and truncated amyloid-β 42(43) deposit in diffuse plaques. Am J Pathol 149: 1823–1830.
40. Johnson MA, Weick JP, Pearce RA, Zhang SC (2007) Functional neural development from human embryonic stem cells: accelerated synaptic activity via astrocyte coculture. J Neurosci 27: 3069–3077.
41. Lazarov O, Lee M, Peterson DA, Sisodia SS (2002) Evidence that synaptically released β-amyloid accumulates as extracellular deposits in the hippocampus of transgenic mice. J Neurosci 22: 9785–9793.
42. Soba P, Eggert S, Wagner K, Zentgraf H, Siehl K, et al. (2005) Homo- and heterodimerization of APP family members promotes intercellular adhesion. EMBO J 24: 3624–3634.
43. Woo SM, Kim J, Han HW, Chae JI, Son MY, et al. (2009) Notch signaling is required for maintaining stem-cell features of neuroprogenitor cells derived from human embryonic stem cells. BMC Neurosci 10: 97.
44. Mangialasche F, Solomon A, Winblad B, Mecocci P, Kivipelto M (2010) Alzheimer's disease: clinical trials and drug development. Lancet Neurol 9: 702–716.
45. Qiang L, Fujita R, Yamashita T, Angulo S, Rhinn H, et al. (2011) Directed conversion of Alzheimer's disease patient skin fibroblasts into functional neurons. Cell 146: 359–371.
46. Kaneko T, Urade Y, Watanabe Y, Mizuno N (1987) Production, characterization, and immunohistochemical application of monoclonal antibodies to glutaminase purified from rat brain. J Neurosci 7: 302–309.
47. Saido TC, Nagao S, Shiramine M, Tsukaguchi M, Sorimachi H, et al. (1992) Autolytic transition of mu-calpain upon activation as resolved by antibodies distinguishing between the pre- and post-autolysis forms. J Biochem 111: 81–86.

ARTHRITIS & RHEUMATISM
Vol. 63, No. 11, November 2011, pp 3625–3632
DOI 10.1002/art.30512

High Incidence of *NLRP3* Somatic Mosaicism in Patients With Chronic Infantile Neurologic, Cutaneous, Articular Syndrome

Results of an International Multicenter Collaborative Study

Naoko Tanaka,[1] Kazushi Izawa,[1] Megumu K. Saito,[2] Mio Sakuma,[3] Koichi Oshima,[4] Osamu Ohara,[4] Ryuta Nishikomori,[1] Takeshi Morimoto,[3] Naotomo Kambe,[5] Raphaela Goldbach-Mansky,[6] Ivona Aksentijevich,[6] Geneviève de Saint Basile,[7] Bénédicte Neven,[8] Mariëlle van Gijn,[9] Joost Frenkel,[9] Juan I. Aróstegui,[10] Jordi Yagüe,[10] Rosa Merino,[11] Mercedes Ibañez,[12] Alessandra Pontillo,[13] Hidetoshi Takada,[14] Tomoyuki Imagawa,[15] Tomoki Kawai,[1] Takahiro Yasumi,[1] Tatsutoshi Nakahata,[2] and Toshio Heike[1]

Objective. **Chronic infantile neurologic, cutaneous, articular (CINCA) syndrome, also known as neonatal-onset multisystem inflammatory disease (NOMID), is a dominantly inherited systemic autoinflammatory disease. Although heterozygous germline gain-of-function *NLRP3* mutations are a known cause of this disease, conventional genetic analyses fail to detect disease-causing mutations in ~40% of patients. Since somatic *NLRP3* mosaicism has been detected in several mutation-negative NOMID/CINCA syndrome patients, we undertook this study to determine the precise contribution of somatic *NLRP3* mosaicism to the etiology of NOMID/CINCA syndrome.**

Methods. **An international case–control study was performed to detect somatic *NLRP3* mosaicism in NOMID/CINCA syndrome patients who had shown no mutation during conventional sequencing. Subcloning and sequencing of *NLRP3* was performed in these mutation-negative NOMID/CINCA syndrome patients and their healthy relatives. Clinical features were analyzed to identify potential genotype–phenotype associations.**

Results. **Somatic *NLRP3* mosaicism was identified in 18 of the 26 patients (69.2%). Estimates of the level of mosaicism ranged from 4.2% to 35.8% (mean ± SD 12.1 ± 7.9%). Mosaicism was not detected in any of the 19 healthy relatives (18 of 26 patients versus 0 of 19**

Supported by Mitsubishi Pharma Research Foundation, the Japanese Ministry of Education, Science, Sports, and Culture, and the Japanese Ministry of Health, Labor, and Welfare.

[1]Naoko Tanaka, MD, Kazushi Izawa, MD, Ryuta Nishikomori, MD, PhD, Tomoki Kawai, MD, Takahiro Yasumi, MD, PhD, Toshio Heike, MD, PhD: Kyoto University Graduate School of Medicine, Kyoto, Japan; [2]Megumu K. Saito, MD, PhD, Tatsutoshi Nakahata, MD, PhD: Center for iPS Cell Research and Application, Kyoto, Japan; [3]Mio Sakuma, MD, PhD, Takeshi Morimoto, MD, PhD: Kyoto University, Kyoto, Japan; [4]Koichi Oshima, MD, Osamu Ohara, PhD: RIKEN Yokohama Institute, Yokohama, Kanagawa, and Kazusa DNA Research Institute, Kisarazu, Chiba, Japan; [5]Naotomo Kambe, MD, PhD: Chiba University Graduate School of Medicine, Chiba, Japan; [6]Raphaela Goldbach-Mansky, MD, Ivona Aksentijevich, MD: National Institute of Arthritis and Musculoskeletal and Skin Diseases, NIH, Bethesda, Maryland; [7]Geneviève de Saint Basile, MD, PhD: Paris Descartes University and INSERM U 768, Paris, France; [8]Bénédicte Neven, MD: Necker Hospital for Sick Children, AP-HP, Paris, France; [9]Mariëlle van Gijn, PhD, Joost Frenkel, MD, PhD: University Medical Centre Utrecht, Utrecht, The Netherlands; [10]Juan I. Aróstegui, MD, PhD, Jordi Yagüe, MD, PhD: Hospital Clínic, Barcelona, Spain; [11]Rosa Merino, MD, PhD: Hospital La Paz, Madrid, Spain; [12]Mercedes Ibañez, MD: Hospital Niño Jesús, Madrid, Spain; [13]Alessandra Pontillo, MD, PhD: IRCCS Burlo Garofalo, Trieste, Italy; [14]Hidetoshi Takada, MD, PhD: Kyushu University Graduate School of Medical Sciences, Fukuoka, Japan; [15]Tomoyuki Imagawa, MD, PhD:Yokohama City University School of Medicine, Yokohama, Kanagawa, Japan.

Drs. Tanaka and Izawa contributed equally to this work.

Dr. Goldbach-Mansky has served as an expert witness on behalf of Biovitrum, Novartis, and Regeneron.

Address correspondence to Osamu Ohara, PhD, Department of Human Genome Research, Kazusa DNA Research Institute, 2-6-7 Kazusakamatari Kisarazu, Chiba 292-0818, Japan (e-mail: ohara@kazusa.or.jp); or to Ryuta Nishikomori, MD, PhD, Department of Pediatrics, Kyoto University Graduate School of Medicine, 54 Shogoin Sakyo, Kyoto 606-8507, Japan (e-mail: rnishiko@kuhp.kyoto-u.ac.jp).

Submitted for publication March 10, 2011; accepted in revised form June 16, 2011.

relatives; $P < 0.0001$). In vitro functional assays indicated that the detected somatic *NLRP3* mutations had disease-causing functional effects. No differences in *NLRP3* mosaicism were detected between different cell lineages. Among nondescript clinical features, a lower incidence of mental retardation was noted in patients with somatic mosaicism. Genotype-matched comparison confirmed that patients with somatic *NLRP3* mosaicism presented with milder neurologic symptoms.

***Conclusion.* Somatic *NLRP3* mutations were identified in 69.2% of patients with mutation-negative NOMID/CINCA syndrome. This indicates that somatic *NLRP3* mosaicism is a major cause of NOMID/CINCA syndrome.**

Chronic infantile neurologic, cutaneous, articular (CINCA) syndrome (MIM no. #607715), also known as neonatal-onset multisystem inflammatory disease (NOMID), is a dominantly-inherited autoinflammatory disease that is characterized by neonatal onset and the triad of urticarial-like skin rash, neurologic manifestations, and arthritis/arthropathy. Patients often experience recurrent fever and systemic inflammation. NOMID/CINCA syndrome is the most severe clinical phenotype of the cryopyrin-associated periodic syndromes (CAPS) that also include the 2 less severe but phenotypically similar syndromes familial cold autoinflammatory syndrome (FCAS; MIM no. #120100) and Muckle-Wells syndrome (MIM no. #191900). CAPS are caused by mutations in the *NLRP3* gene, which is a member of the nucleotide-binding oligomerization domain–like receptor (NLR) family of the innate immune system (1,2).

NLRP3 is an intracellular "sensor" of danger signals arising from cellular insults, such as infection, tissue damage, and metabolic deregulation, and it has been highly conserved throughout evolution. NLRP3 associates with ASC and procaspase 1 to constitute a large multiprotein complex termed the NLRP3 inflammasome. When activated, the NLRP3 inflammasome converts the biologically inactive procaspase 1 into active caspase 1. Caspase 1 produces the cytokines interleukin-1β (IL-1β) and IL-18, which are mainly involved in the inflammatory response (3). Available research suggests that mutated *NLRP3* induces autoactivation of the NLRP3 inflammasome in CAPS patients, resulting in an uncontrolled overproduction of IL-1β.

Most CAPS patients carry heterozygous germline missense mutations in the *NLRP3* coding region ("mutation-positive" patients) (4,5). More than 80 different disease-causing mutations have been reported to date (6). However, ~40% of clinically diagnosed NOMID/CINCA syndrome patients show no heterozygous germline *NLRP3* mutation during conventional Sanger-sequencing-based genetic analyses ("mutation-negative" patients). Comparisons of NOMID/CINCA syndrome patients with and without heterozygous germline *NLRP3* mutations have revealed no differences in clinical features or response to treatment (4,7).

In a previous study, we identified a high incidence of somatic *NLRP3* mosaicism in "mutation-negative" NOMID/CINCA syndrome patients in Japan (8). We therefore hypothesized that somatic *NLRP3* mosaicism may be implicated in the etiology of the disorder, although its precise contribution remains unclear. The aim of the present study was to evaluate both the frequency of *NLRP3* somatic mosaicism in NOMID/CINCA syndrome patients and the association between somatic mosaicism and clinical phenotype using an international cohort of mutation-negative NOMID/CINCA syndrome patients.

PATIENTS AND METHODS

Study design and participants. International collaborators were contacted to identify mutation-negative NOMID/CINCA syndrome cases. A total of 20 DNA samples were received from 4 centers: France (n = 6), The Netherlands (n = 4), Spain (n = 3), and the US (n = 7). DNA samples had been extracted from peripheral blood mononuclear cells or whole blood. All 20 samples had been subjected to conventional sequencing, and no *NLRP3* mutations had been identified. In each case, the accuracy of the clinical diagnosis had been confirmed according to the diagnostic criteria (7). The 6 previously reported Japanese cases and 1 Spanish case with *NLRP3* somatic mosaicism were also included (8,9). DNA samples were also collected from 19 healthy relatives of 8 patients (8 from France, 5 from Japan, 2 from Spain, and 4 from the US) to evaluate the causality of somatic *NLRP3* mosaicism in a case–control manner, since the clinical features may be modified by genetic and environmental factors.

Written informed consent for *NLRP3* gene analysis was obtained from all patients and controls. The study was approved by the Institutional Review Board of the Kyoto University Graduate School of Medicine and was conducted in accordance with the Declaration of Helsinki.

Data collection. *Demographic and clinical data.* The clinicians responsible for each mutation-negative NOMID/CINCA syndrome patient completed a questionnaire to document characteristics such as age, sex, race, symptoms, clinical findings, clinical course, and prognosis. No clinical data were obtained from the healthy controls.

Investigation of NLRP3 gene mosaicism. Disease-causing mutations in NOMID/CINCA syndrome patients have

only been reported in exons 3, 4, and 6 of *NLRP3* (6). Thus, the present sequencing was focused on a search for somatic mosaicism of these 3 exons and their flanking intronic regions. After amplifying these genomic regions with the proofreading polymerase chain reaction (PCR) enzyme KOD-Plus polymerase (Toyobo) and dA addition with an LA *Taq* polymerase (Takara Bio), the amplicons were subcloned into pCR2.1-TOPO vector (Invitrogen). Ninety-six clones were selected at random for each amplicon. The subcloned amplicons were retrieved by PCR with LA *Taq* polymerase. They were then treated with ExoSAP-IT (USB) and proteinase K (Promega) prior to direct sequencing. The cloned exons were sequenced at the Kazusa DNA Research Institute using a BigDye Terminator kit (version 3.1) and an ABI 3730 DNA sequencer (Life Technologies). Mosaicism was indicated by the detection of >2 subclones carrying the same base variation at the same position in 96 clones.

To purify leukocyte subpopulations, freshly drawn whole blood was separated using sequential dextran and Ficoll-Hypaque density-gradient centrifugation methods. Cell sorting to select T cells, B cells, and monocytes was performed with an AutoMACS Pro Separator (Miltenyi Biotec) or a FACSVantage System (BD Biosciences), as described elsewhere (8,9). The purity of each cell lineage was >90%. The level of mosaicism was determined by sequencing each source of genomic DNA from 80 clones.

Plasmids and cell lines. To determine whether the identified NLRP3 mutants cause disease, experiments for assessing 2 pathologic functions were performed as described elsewhere (8). Briefly, ASC-dependent NF-κB activation was performed by a dual-luciferase reporter assay in HEK 293FT cells transfected with NLRP3 mutants. Transfection-induced cell death in the human monocytic cell line THP-1 was performed by transfecting green fluorescent protein–fused mutant NLRP3 into THP-1 cells and then measuring the dead cells with 7-aminoactinomycin D.

Statistical analysis. The study was designed to detect mosaicism at a 5% allele frequency with >95% possibility. To satisfy this condition, it was necessary to sequence at least 93 clones per patient. The following calculation was used to estimate the number of clones that had to be sequenced: $P = 1 - (1 - 0.05)^n - n(0.05)(1 - 0.05)^{n-1}$ ($n = 93$, $P = 0.956$). The study was designed to analyze 96 PCR-fragment clones from each patient. The error rate of the PCR reactions was estimated using a proofreading KOD-Plus enzyme. We analyzed a plasmid vector carrying a normal *NLRP3* exon 3, in which 2 distinct errors were detected by sequencing 91 clones. The calculated error rate for this result was 1/87,451 (2/[1,922 bp × 91 clones]). Thus, the probability was negligible that the same errors would be detected more than twice in 96 clones from 1 patient.

To calculate the sample size, we calculated the prevalence of somatic mosaicism among mutation-negative NOMID/CINCA syndrome patients. Eight cases of somatic mosaicism were identified among 15 mutation-negative NOMID/CINCA syndrome patients who were subsequently analyzed by the subcloning method described above. It was assumed that the maximum number of possible somatic mosaicism cases among family controls was 1. On the basis of these data and this assumption, it was calculated that 19 controls were required to ensure a 2-sided alpha level of 0.05 and a power of 0.8.

Continuous variables are presented as the mean ± SD or as the median and interquartile range. Categorical variables are presented as numbers and ratios (with percentages). To compare clinical data between patients with and patients without mosaicism, the Wilcoxon rank sum test was used for continuous variables and Fisher's exact test was used for categorical variables. Fisher's exact test was used to compare the difference in mosaicism ratio between cases and controls. The chi-square test was used to compare the difference in the level of mosaicism between different sources of genomic DNA from each patient.

Table 1. Somatic mosaicism among mutation-negative NOMID/CINCA syndrome patients*

Country, patient	Sequence variant	Protein variant	Mosaicism, %
France			
F1	1298C>T	T433I	5.2
F2	907G>C	D303H	4.2
F3	1315G>C	A439P	21.9
F4	1216A>G	M406V	9.2
F5	1698C>A	F566L	11.5
F6	None	–	–
Japan			
J1	1709A>G	Y570C	12.2
J2	790C>T	L264F	4.3
J3	919G>A	G307S	10.7
J4	1699G>A	E567K	6.5
J5	907G>C	D303H	11.9
J6	None	–	–
Spain			
S1	920G>T	G307V	9.6
S2	907G>C	D303H	19.1
S3	None	–	–
S4	None	–	–
US			
A1	1065A>T	K355N	18.8
A2	1698C>A	F566L	14.6
A3	1704G>C	K568N	9.4
A4	2263G>A	G755R	35.8
A5	None	–	–
A6	None	–	–
The Netherlands			
N1	1699G>A	E567K	6.3
N2	2263G>A	G755R	6.3
N3	None	–	–
N4	None	–	–

* *NLRP3* mosaicism was detected in 18 of 26 patients (69.2%) with neonatal-onset multisystem inflammatory disease (NOMID)/chronic infantile neurologic, cutaneous, articular syndrome (CINCA syndrome). When samples from 19 healthy relatives of these patients were investigated, no somatic mosaicism was detected. The *P* value from the comparison of the cases and the controls (18 of 26 versus 0 of 19) was statistically significant ($P < 0.0001$).

RESULTS

Somatic *NLRP3* mosaicism in mutation-negative NOMID/CINCA syndrome patients. A heterozygous germline *NLRP3* mutation was detected in 1 of the 27 samples, and this was therefore excluded from the analyses. For each patient, 96 clones were selected at random for each amplicon. These were then sequenced. *NLRP3* mosaicism was detected in 18 of 26 patients (69.2%), and the level of allelic mosaicism ranged from 4.2% to 35.8% (mean ± SD 12.1 ± 7.9%; median 10.2%) (Table 1). Seven of the detected *NLRP3* mutations were novel (p.G307S, p.K355N, p.M406V, p.T433I, p.F566L, p.E567K, and p.K568N). The remaining mutations have been reported previously in NOMID/CINCA syndrome patients as disease-causing heterozygous germline mutations (p.L264F, p.D303H, p.G307V, p.A439P, p.Y570C, and p.G755R). Each of the 3 *NLRP3* mutations, p.F566L, p.E567K, and p.G755R, was detected in 2 unrelated patients. *NLRP3* mutation p.D303H was detected in 3 unrelated patients.

Analyses in family controls. To validate the clinical relevance of the *NLRP3* mosaicism identified in mutation-negative NOMID/CINCA syndrome patients, samples from 19 healthy relatives were investigated. No somatic mosaicism was detected in any of these samples. The *P* value from the comparison of cases and controls (18 of 26 versus 0 of 19) was statistically significant ($P < 0.0001$).

Functional effects of the identified somatic *NLRP3* mutations. Since disease-causing heterozygous germline mutations in *NLRP3* have been implicated in necrosis-like programmed cell death and ASC-dependent NF-κB activation (8), experiments were performed to determine whether the mutations identified in patients with somatic mosaicism showed the same effects. All of the identified mutations induced both THP-1 cell death (Figure 1A) and ASC-dependent NF-κB activation (Figure 1B). The in vitro effects of these novel mutations were similar to or even more pronounced than those of previously reported *NLRP3* mutations. This strongly suggests that all mutations showing somatic mosaicism have pathogenic effects, including the novel mutations identified in the present study.

Mutation frequency of *NLRP3* among various cell lineages and 1 tissue type. To explore the origin of the *NLRP3* mosaicism, mutational frequency was evaluated in various cell lineages and 1 tissue type from 4 Japanese patients with *NLRP3* somatic mosaicism. In each patient, the same mutations were found in all of the cell lineages investigated (neutrophils, monocytes, T cells, B cells) and in the buccal mucosa tissue, and no significant difference in mutation frequency was observed between these sources (Table 2).

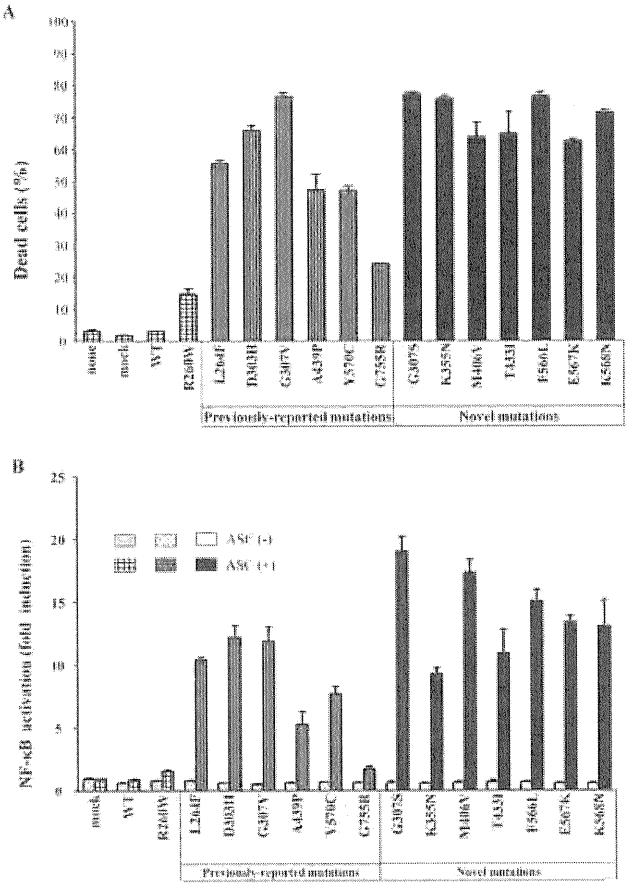

Figure 1. In vitro functional assessment of the identified *NLRP3* mosaicism mutations. **A,** Necrotic cell death of THP-1 cells induced by the identified somatic *NLRP3* mosaicism mutations. Green fluorescent protein (GFP)–fused mutant NLRP3 was transfected into THP-1 cells. The percentage of dead cells (7-aminoactinomycin D positive) among GFP-positive cells is shown. Values are the mean ± SD of triplicate experiments, and data are representative of 2 independent experiments. None = nothing transfected; mock = vector without NLRP3; WT = wild-type NLRP3; R260W = NLRP3 with p.R260W (frequent mutations in patients with cryopyrin-associated periodic syndromes). **B,** ASC-dependent NF-κB activation induced by the identified somatic *NLRP3* mosaicism mutations. HEK 293FT cells were cotransfected with WT or mutant NLRP3 in the presence or absence of ASC. The induction of NF-κB is shown as the fold change compared with cells that were transfected with a control vector without ASC (set at 1). Values are the mean ± SD of triplicate experiments, and data are representative of 2 independent experiments.

Table 2. Distribution and quantification of *NLRP3* mutations among sources of genomic DNA (4 cell lineages and 1 tissue type)*

Patient	Sequence variant	Protein variant	Mosaicism, %				
			Neutrophils	Monocytes	T cells	B cells	Buccal mucosa
J1	1709A>G	Y570C	12.6	9.8	8.0	9.5	8.3
J3	919G>A	G307S	9.1	10.8	6.9	10.6	9.0
J4	1699G>A	E567K	3.5	2.3	3.7	3.4	2.2
J5	907G>C	D303H	14.4	8.7	7.7	8.5	13.5

* No significant differences in the level of mosaicism were observed among the sources of genomic DNA.

Phenotype–genotype analysis. Given the previously reported genotype–phenotype association between the *NLRP3* gene and CAPS, the clinical characteristics of NOMID/CINCA syndrome patients with somatic *NLRP3* mutations were compared with those of patients from previous reports who had the same *NLRP3* mutations but with heterozygous germline status (1,4,10–13) (Figure 2) (further information is available at http://web16.kazusa.or.jp/download/). All of the patients in these 2 groups had an early onset of the disease, fever, and urticarial rash. The presence of arthritis, bony overgrowth, contractures, hearing loss, and seizure varied in each group of patients, and no significant difference was detected. However, whereas most patients with heterozygous germline *NLRP3* mutations presented with mental retardation, this was not the case for patients with somatic *NLRP3* mosaicism. A comparison was also made between the clinical data from patients with somatic *NLRP3* mosaicism and the data from patients with neither germline nor somatic *NLRP3* mutations. Again, a lower incidence of mental retardation was observed in patients with somatic *NLRP3* mosaicism

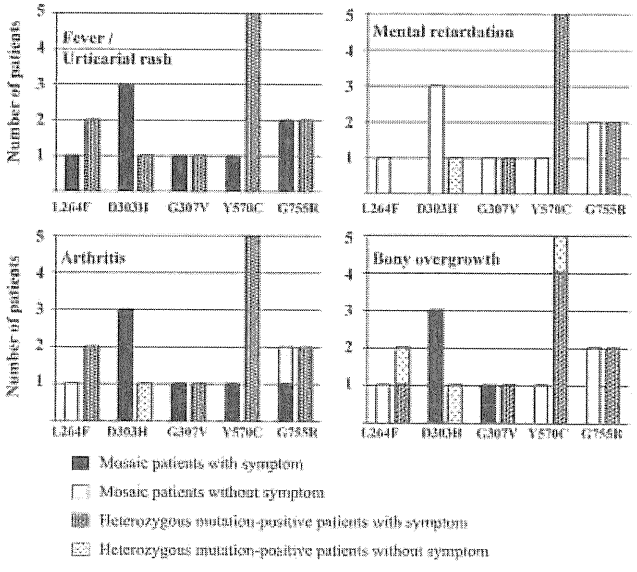

Figure 2. Comparison of the clinical profiles of patients carrying somatic *NLRP3* mutations and patients carrying the same mutation, but with germline status. Clinical profiles of patients with mosaicism and those of patients with heterozygous germline mutations are compared for each protein variant (L264F, D303H, G307V, Y570C, and G755R). The data on 4 typical clinical symptoms are shown. Total numbers of patients with mosaicism and total numbers of patients with heterozygous mutation examined are shown as a bar for each protein variant. Each bar is stratified according to the presence or absence of the symptom. For the protein variant L264F, no data on mental retardation were available for the patient with a heterozygous germline mutation.

Table 3. Clinical profiles of patients with somatic *NLRP3* mosaicism and patients with neither germline nor somatic *NLRP3* mutations*

	Patients with somatic *NLRP3* mosaicism (n = 18)	Patients with neither germline nor somatic *NLRP3* mutations (n = 8)
Age, median (IQR) years	12 (1–30)	10 (3–21)
No. of men/women	10/8	3/5
Age at onset, median (IQR) months	0 (0–24)	0.5 (0–33)
Fever	17/17	7/7
Urticarial rash	14/14	8/8
Mental retardation	4/17	6/8
Meningitis	13/17	5/8
Seizures	2/18	1/7
Hearing loss	10/18	2/7
Arthritis	14/17	7/8
Bony overgrowth	12/17	6/7
Contractures	7/17	4/7
Walking disability	8/18	3/7
Biologic therapy	10/15	3/8

* Except where indicated otherwise, values are the number with the feature/the total number of patients assessed. A lower incidence of mental retardation was observed in patients with somatic *NLRP3* mosaicism ($P = 0.03$). No other significant differences were detected between the groups. IQR = interquartile range.

($P = 0.03$). No other significant differences were detected (Table 3) (further information is available at http://web16.kazusa.or.jp/download/).

DISCUSSION

The present international multicenter study investigated 26 NOMID/CINCA syndrome patients who were mutation negative according to conventional sequencing along with 19 family controls to determine whether low-level mosaicism is a disease-causing genetic mechanism. Following our first report of low-level somatic mosaicism in a NOMID/CINCA syndrome patient (14), we reported a new method of detecting low-level *NLRP3* mosaicism, in which lipopolysaccharide (LPS) induced cell death specifically in *NLRP3* mutation–positive monocytes (8). However, this method requires fresh live monocytes, special equipment such as a cell sorter, and experience in its use due to the rapid time course of LPS-induced necrotic monocytic death. For these reasons, application of this method was not feasible in an international collaborative study. We therefore opted to use genomic DNA, since it is easier to handle and can be stored and shipped. Based on our previous study in Japanese patients showing that the frequency of mutant alleles could be <5%, we designed a subcloning and Sanger-sequencing strategy that could detect this very low allelic mutation frequency.

Presuming that the present cohort is representative of the 40% of NOMID/CINCA syndrome patients who are mutation negative according to conventional sequencing, the results suggest that ~28% of all NOMID/CINCA syndrome patients may carry somatic *NLRP3* mosaicism. CAPS patients present with a continuous spectrum of symptoms, and a degree of genotypic overlap is observed between disease subtypes. Although the present study focused on the most severe NOMID/CINCA syndrome phenotype, it is possible that somatic *NLRP3* mosaicism may also occur in milder forms of CAPS. The presence of somatic mosaicism should also be investigated in patients with other dominantly inherited autoinflammatory diseases caused by gain-of-function mutations and who are mutation negative according to conventional sequencing.

Among the 18 patients with somatic *NLRP3* mosaicism, we found 6 mutations that have previously been identified in NOMID/CINCA syndrome patients as heterozygous germline mutations. We also identified 7 novel mutations, which were confirmed as being functionally active and presumably pathogenic. Functional in vitro assays showed that these novel mutations had greater disease-causing capacity than the previously described mutations. This suggests that the novel mutations may be deleterious and unrecognized if inherited as heterozygous germline mutations.

The present study also addressed the important question of how somatic *NLRP3* mosaicism modifies clinical presentation. Although no statistically significant differences in age at disease onset, skin symptoms, joint involvement, or response to IL-1 blockade were detected, milder neurologic involvement was observed in patients with somatic mosaicism. Comparisons with NOMID/CINCA syndrome patients carrying the same *NLRP3* mutations but with heterozygous germline status made this tendency more prominent. Although the level of somatic mosaicism in blood leukocytes was relatively low, it remains unclear how these low-level mutations influence clinical presentation, including disease severity. One interesting hypothesis is that the difference in the severity of neurologic manifestations is a function of the level of mosaicism. For ethical and technical reasons, it was not possible to evaluate the level of mosaicism in central nervous system (CNS) cells or glial cells in the present study, and this therefore awaits investigation in future studies.

The mechanism through which *NLRP3* somatic mosaicism occurs also requires elucidation. The present study demonstrated that similar proportions of neutrophils, T cells, B cells, monocytes, and buccal cells carried the mutated allele. Therefore, the mutation leading to mosaicism must have arisen before the pluripotent stem cells committed to hematopoietic progenitor stem cells or ectoderm-derived nonhematopoietic cells. Several mechanisms for mosaicism have been proposed, including chimerism due to cell fusion with an aborted dizygotic twin and a mutational event during early embryogenesis (15). The latter mechanism is more likely in the present cohort, since mosaicism at similar frequency was detected in several cell types. To verify the hypothesis of a mutational event during embryogenesis, and to determine the point at which this occurred, it would be helpful to analyze other tissues. However, obtaining such tissues from patients may be ethically problematic.

Approximately 12% of the patients in the present cohort carried neither germline nor somatic *NLRP3* mutations and may therefore be considered to be genuinely mutation negative. However, it is possible that these patients have *NLRP3* mutations that have been overlooked. A recent report described a mutation in the 5′-untranslated region of *NLRP3* in a patient with FCAS

(16), although it remains unclear how this noncoding mutation causes disease. Another possibility is that an extremely low frequency of NLRP3 mosaicism may have been missed. The subcloning and Sanger-sequencing strategy used in this study set the detection limit of mosaicism at 5%. Considering the range of *NLRP3* mosaicism detected (4.2–35.8%), the median (10.2%), and the identification of 2 patients with <5% mosaicism, it is indeed likely that patients with an even lower level of *NLRP3* mosaicism may have been overlooked. Recent advances in next-generation DNA sequencing technology may resolve this technical problem, although the associated error rate could be problematic. Another possibility is that *NLRP3* mutations were present in uninvestigated cell lineages, such as those from CNS tissue, bone tissue, or skin. Future studies of NOMID/CINCA syndrome should investigate these tissues while searching for mutations in other genes.

In conclusion, the present study has clearly demonstrated that a significant proportion of NOMID/CINCA syndrome patients who were mutation negative according to conventional sequencing carried somatic *NLRP3* mutations with a variable degree of mosaicism. Clinicians should therefore consider somatic mosaicism as a possible cause of disease in mutation-negative NOMID/CINCA syndrome patients and implement appropriate therapy. The early diagnosis of NOMID/CINCA syndrome and prompt initiation of therapy would improve clinical outcome. Further goals in this research field are the refinement of genetic screening and the verification of the functional consequences of all detected somatic mutations. Systematic screening for somatic mosaicism will provide new insights into the etiology of human disease.

ACKNOWLEDGMENTS

We thank all patients and their relatives for participating in the study. We are grateful to Yuki Takaoka at the Department of Pediatrics, Kyoto University Graduate School of Medicine and Seiko Watanabe at the Department of Human Genome Research, Kazusa DNA Research Institute for their technical assistance.

AUTHOR CONTRIBUTIONS

All authors were involved in drafting the article or revising it critically for important intellectual content, and all authors approved the final version to be published. Drs. Ohara and Nishikomori had full access to all of the data in the study and take responsibility for the integrity of the data and the accuracy of the data analysis.

Study conception and design. Saito, Ohara, Nishikomori, Kambe.

Acquisition of data. Tanaka, Izawa, Saito, Oshima, Ohara, Nishikomori, Goldbach-Mansky, Aksentijevich, de Saint Basile, Neven, van Gijn, Frenkel, Aróstegui, Yagüe, Merino, Ibañez, Pontillo, Takada, Imagawa.

Analysis and interpretation of data. Sakuma, Morimoto, Kawai, Yasumi, Nakahata, Heike.

ROLE OF THE STUDY SPONSOR

Mitsubishi Pharma Research Foundation supported the data collection for this study, approved the contents of the manuscript, and agreed to submit the manuscript for publication.

REFERENCES

1. Neven B, Callebaut I, Prieur AM, Feldmann J, Bodemer C, Lepore L, et al. Molecular basis of the spectral expression of CIAS1 mutations associated with phagocytic cell-mediated autoinflammatory disorders CINCA/NOMID, MWS, and FCU. Blood 2004;103:2809–15.
2. Stojanov S, Kastner DL. Familial autoinflammatory diseases: genetics, pathogenesis and treatment. Curr Opin Rheumatol 2005; 17:586–99.
3. Schroder K, Zhou R, Tschopp J. The NLRP3 inflammasome: a sensor for metabolic danger? Science 2010;327:296–300.
4. Aksentijevich I, Nowak M, Mallah M, Chae JJ, Watford WT, Hofmann SR, et al. De novo CIAS1 mutations, cytokine activation, and evidence for genetic heterogeneity in patients with neonatal-onset multisystem inflammatory disease (NOMID): a new member of the expanding family of pyrin-associated autoinflammatory diseases. Arthritis Rheum 2002;46:3340–8.
5. Hoffman HM, Mueller JL, Broide DH, Wanderer AA, Kolodner RD. Mutation of a new gene encoding a putative pyrin-like protein causes familial cold autoinflammatory syndrome and Muckle-Wells syndrome. Nat Genet 2001;29:301–5.
6. Milhavet F, Cuisset L, Hoffman HM, Slim R, El-Shanti H, Aksentijevich I, et al. The Infevers autoinflammatory mutation online registry: update with new genes and functions. Hum Mutat 2008;29:803–8.
7. Goldbach-Mansky R, Dailey NJ, Canna SW, Gelabert A, Jones J, Rubin BI, et al. Neonatal-onset multisystem inflammatory disease responsive to interleukin-1β inhibition. N Engl J Med 2006;355: 581–92.
8. Saito M, Nishikomori R, Kambe N, Fujisawa A, Tanizaki H, Takeichi K, et al. Disease-associated CIAS1 mutations induce monocyte death, revealing low-level mosaicism in mutation-negative cryopyrin-associated periodic syndrome patients. Blood 2008;111:2132–41.
9. Arostegui JI, Lopez Saldana MD, Pascal M, Clemente D, Aymerich M, Balaguer F, et al. A somatic NLRP3 mutation as a cause of a sporadic case of chronic infantile neurologic, cutaneous, articular syndrome/neonatal-onset multisystem inflammatory disease: novel evidence of the role of low-level mosaicism as the pathophysiologic mechanism underlying Mendelian inherited diseases. Arthritis Rheum 2010;62:1158–66.
10. Rosen-Wolff A, Quietzsch J, Schroder H, Lehmann R, Gahr M, Roesler J. Two German CINCA (NOMID) patients with different clinical severity and response to anti-inflammatory treatment. Eur J Haematol 2003;71:215–9.
11. Aksentijevich I, Putnam CD, Remmers EF, Mueller JL, Le J, Kolodner RD, et al. The clinical continuum of cryopyrinopathies: novel CIAS1 mutations in North American patients and a new cryopyrin model. Arthritis Rheum 2007;56:1273–85.
12. Matsubayashi T, Sugiura H, Arai T, Oh-Ishi T, Inamo Y. Anakinra

therapy for CINCA syndrome with a novel mutation in exon 4 of the CIAS1 gene. Acta Paediatr 2006;95:246–9.
13. Jesus AA, Silva CA, Segundo GR, Aksentijevich I, Fujihira E, Watanabe M, et al. Phenotype–genotype analysis of cryopyrin-associated periodic syndromes (CAPS): description of a rare non-exon 3 and a novel CIAS1 missense mutation. J Clin Immunol 2008;28:134–8.
14. Saito M, Fujisawa A, Nishikomori R, Kambe N, Nakata-Hizume M, Yoshimoto M, et al. Somatic mosaicism of CIAS1 in a patient with chronic infantile neurologic, cutaneous, articular syndrome. Arthritis Rheum 2005;52:3579–85.
15. Erickson RP. Somatic gene mutation and human disease other than cancer: an update. Mutat Res 2010;705:96–106.
16. Anderson JP, Mueller JL, Misaghi A, Anderson S, Sivagnanam M, Kolodner RD, et al. Initial description of the human NLRP3 promoter. Genes Immun 2008;9:721–6.

特集
小児医療における診断・治療の進歩　22
治療技術

Key words
induced pluripotent stem（iPS）細胞
臨床応用
疾患特異的 iPS 細胞
遺伝子治療
個別化医療

疾患特異的 iPS 細胞を用いた遺伝子治療・個別化医療

中畑 龍俊（なかはた たつとし）*

要旨

山中教授らにより成熟した細胞にたった 4 つの転写因子遺伝子を導入することにより作製されたヒト iPS 細胞は，未分化な状態のままほぼ無限に増やすことができ，われわれの身体を構成するすべての細胞への多分化能を有することから，幅広い医療への応用が期待されている．iPS 細胞のもつもっとも画期的な臨床的側面は，さまざまな疾患の患者から皮膚などの組織を用いて疾患特異的 iPS 細胞を樹立できることである．この細胞を用いて，診断，疾患の病態解析，新規治療法の開発，新規薬剤の有効性・毒性の検定などに応用されると考えられる．将来的には患者 iPS 細胞は異常遺伝子を修復した遺伝子治療と複合した再生医療や個別化医療への応用が期待されている．

はじめに

ヒト受精卵を滅失して樹立される ES 細胞は，社会的，倫理的に多くの問題を抱えているが，ほぼ無限に増殖でき，さまざまな細胞に *in vitro* で分化可能であることから，幅広い再生医療への応用が期待され，米国では昨年ヒト ES 細胞を用いた再生医療が開始された．人工多能性幹細胞（induced pluripotent stem cell：iPS 細胞）は受精卵を破壊することなく同様な能力を持った細胞を健常人や患者自身の皮膚や血液から作製可能なことから，再生医療への応用のみならず疾患解析や新規治療法の開発に応用されている．本稿では疾患特異的 iPS 細胞を中心にその遺伝子治療や個別化医療への応用について概説した．

* 京都大学 iPS 細胞研究所，臨床応用研究部門
〒 606-8507 京都府京都市左京区聖護院川原町 53

Ⅰ 人工多能性幹細胞（iPS 細胞）

2006 年，山中ら[1]はレトロウイルスベクターを用いてマウス胎児線維芽細胞に Oct3/4，Sox2，Klf4，および c-Myc というたった 4 つの転写因子遺伝子を導入することにより，ES 細胞と比べても遜色がない能力を持つ iPS 細胞の樹立に成功し，世界中に大きな衝撃を与えた．iPS 細胞は ES 細胞特異的なマーカーを発現するようになり，*in vitro*，*in vivo* で三胚葉系の細胞に分化することができ，さらにキメラマウスを作出することも可能であったことから，ES 細胞と同等の機能を獲得したものであると考えられた．翌年，彼らはヒト皮膚線維芽細胞にマウスと同様の 4 つの遺伝子を導入することによりヒト iPS 細胞の樹立に成功した（図 1）[2]．

ヒト iPS 細胞は，受精卵を滅失することなく作製できることから，ヒト ES 細胞の持つ社会的，倫理的な多くの問題を回避することができ

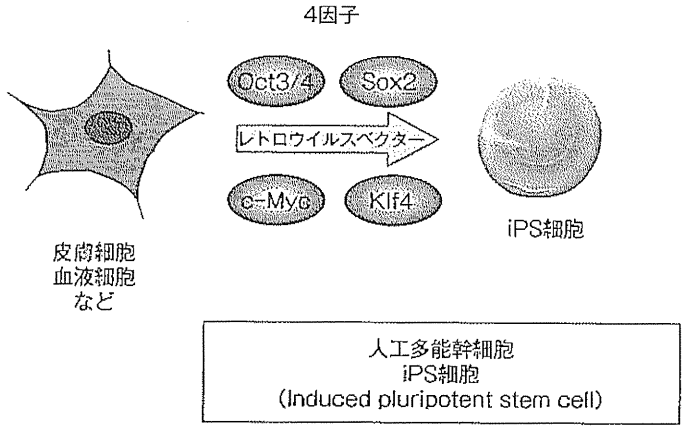

図1 ヒトiPS細胞の誘導

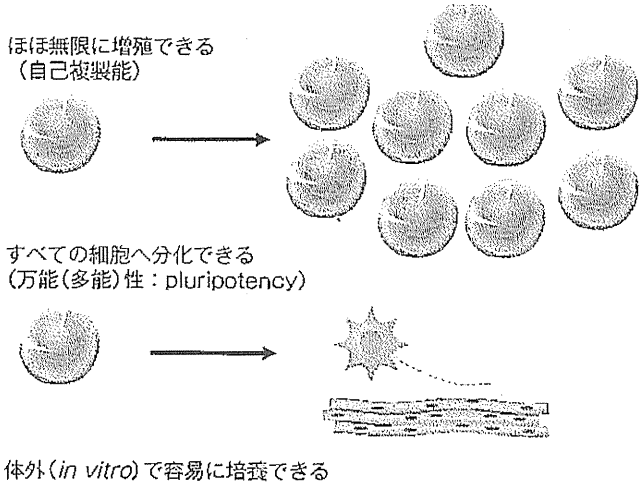

図2 iPS細胞の特性

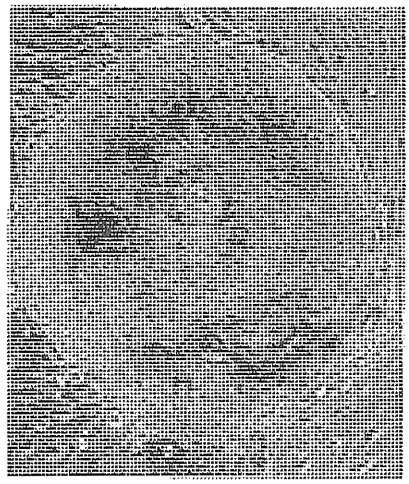

図3 ある患者から樹立されたiPS細胞
細胞が密に接触しながら増殖している.

る．ヒトiPS細胞はES細胞と同様に未分化な状態のままほぼ無限に増やせること，培養条件を変化させると，神経細胞，心筋，骨格筋，血管内皮細胞，軟骨や骨の細胞，膵島細胞，肝細胞，各種血液細胞などさまざまな細胞に*in vitro*で分化可能であることから，幅広い再生医療や遺伝子治療への応用が期待されている（図2）．臨床応用可能な，より安全性の高いiPS細胞を樹立するためさまざまな検討が行われている．

当初，皮膚線維芽細胞から樹立されていたiPS細胞はその後，骨髄細胞，臍帯血，末梢血，毛根細胞，歯髄細胞，脂肪組織などさまざまな組織から樹立可能となり，どの組織を材料にして作製したiPS細胞がもっとも優れているか検討が行われている．

当初Oct3/4, Sox2, Klf4, c-Mycの4つの転写因子遺伝子を導入してiPS細胞の樹立が行われていたが，最近ではがん遺伝子でもあるc-